

Review

A Critical Review of Ultrasonic-Assisted Machining of Titanium Alloys

Muhammad Fawad Jamil , Qilin Li, Mohammad Keymanesh, Pingfa Feng  and Jianfu Zhang * 

State Key Laboratory of Tribology in Advanced Equipment, Department of Mechanical Engineering, Tsinghua University, Beijing 100084, China; jme23@mails.tsinghua.edu.cn (M.F.J.); liqilin_thu@mail.tsinghua.edu.cn (Q.L.); keymaneshm10@mails.tsinghua.edu.cn (M.K.); fengpf@mail.tsinghua.edu.cn (P.F.)

* Correspondence: zhjf@tsinghua.edu.cn

Abstract

Ultrasonic-assisted machining (UAM) has emerged as a transformative technology for increasing material removal efficiency, improving surface quality and extending tool life in precision manufacturing. This review specifically focuses on the application of it to titanium aluminide (TiAl) alloys. These alloys are widely used in aerospace and automotive sectors due to their low density, high strength and poor machinability. This review covers various aspects of UAM, including ultrasonic vibration-assisted turning (UVAT), milling (UVAM) and grinding (UVAG), with emphasis on their influence on the machinability, tool wear behavior and surface integrity. It also highlights the limitations of single-energy field UAM, such as inconsistent energy transmission and tool fatigue, leading to the increasing demand for multi-field techniques. Therefore, the advanced machining strategies, i.e., ultrasonic plasma oxidation-assisted grinding (UPOAG), protective coating-assisted cutting, and dual-field ultrasonic integration (e.g., ultrasonic-magnetic or ultrasonic-laser machining), were discussed in terms of their potential to further improve TiAl alloys processing. In addition, the importance of predictive force models in optimizing UAM processes was also highlighted, emphasizing the role of analytical and AI-driven simulations for better process control. Overall, this review underscores the ongoing evolution of UAM as a cornerstone of high-efficiency and precision manufacturing, while providing a comprehensive outlook on its current applications and future potential in machining TiAl alloys.



Academic Editor: Kai Cheng

Received: 22 July 2025

Revised: 29 August 2025

Accepted: 9 September 2025

Published: 11 September 2025

Citation: Jamil, M.F.; Li, Q.; Keymanesh, M.; Feng, P.; Zhang, J. A Critical Review of Ultrasonic-Assisted Machining of Titanium Alloys. *Machines* **2025**, *13*, 844. <https://doi.org/10.3390/machines13090844>

Copyright: © 2025 by the authors. Licensee MDPI, Basel, Switzerland. This article is an open access article distributed under the terms and conditions of the Creative Commons Attribution (CC BY) license (<https://creativecommons.org/licenses/by/4.0/>).

Keywords: γ -TiAl; additive manufacturing; ultrasonic-assisted machining; multi-energy field; predictive models

1. Introduction

Intermetallic alloys of titanium and aluminum have always been a subject of growing interest due to their unique combination of high-temperature strength, low density, fatigue resistance [1] and excellent corrosion resistance [2,3]. Due to such properties, they are ideal materials for aerospace [4], defense and medical industry [5,6] applications. However, their brittle nature at room temperature poses significant challenges in machining [7,8]. This is due to the highly versatile combinations of alloying elements tailored for specific applications. The emergence of multi-component alloys, i.e., Ti-Al-Nb, Ti-Al-V and Ti-Al-Si, has significantly expanded their potential [9]. The ongoing research is crucial to overcoming these barriers for broader industrial adoption.

Ultrasonic-assisted machining (UAM) has emerged as a superior alternative to conventional machining (CM) for advanced materials (i.e., γ -TiAl intermetallic alloys) [10,11].

It enhances the cutting performance due to high-frequency and small-amplitude vibrations [12]. Yang et al.'s [13] study comprehensively reviews the evolution of UAM systems, from 1D to 3D configurations and analysis kinematics based on tool/workpiece motion. Key cutting characteristics such as contact rate, cutting force and surface integrity were summarized, highlighting the advantages in reducing machining forces. Despite these benefits, challenges remain in developing high-power, large-amplitude and efficient ultrasonic systems, as well as advancing theoretical research on UAM dynamics [14]. Given its interdisciplinary nature, future advancements should focus on the processing innovations and theoretical breakthroughs to further optimize UAM capabilities for intermetallic alloys applications in aerospace, medical and defense industry, as shown in Figure 1.

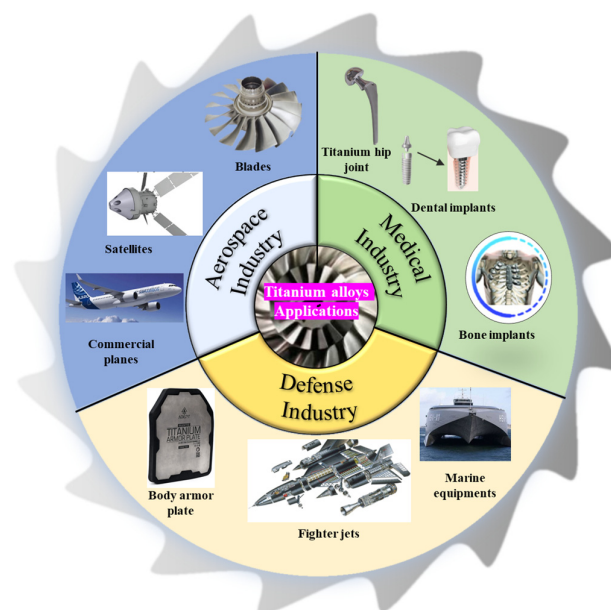


Figure 1. Applications of intermetallic titanium alloys in aerospace, medical and defense sectors.

The literature selection process was structured following a PRISMA-style approach. Figure 2a summarizes the identification, screening, eligibility and inclusion strategies applied to TiAl machining studies. The distribution of literature in the field of machining and post-processing of titanium alloys reveals a clear dominance of studies focused on grinding, accounting for more than 50% of the total publications as shown in Figure 2b. The data were obtained through a comprehensive literature survey conducted using major scientific databases including Scopus, Web of Science, Springer and ScienceDirect. The search covered publications from the past two decades, with a main focus on 2017–25, using keywords such as “machining of titanium alloys”, “post-processing of titanium alloys”, “grinding titanium alloys” and related terms. Relevant articles were filtered based on their focus on specific machining or post-processing techniques and the final distribution was categorized accordingly. This distribution suggested that the researchers have extensively explored the effects of ultrasonic vibration-assisted turning (UVAT), milling (UVAM) and grinding (UVAG). Figure 2c shows the distribution of these studies over the past decade and underscores the importance and preference for high-frequency vibrations.

The present research primarily focuses on technological advancements and processing methods that integrate UAM to overcome machining challenges. In this paper, Section 2 discusses the characterization and processing considerations for TiAl. Section 3 is focused on the machining efficiency of TiAl with particular emphasis on various types of UAM (i.e., UVAM, UVAT and UVAG). The focus is on major key aspects: cutting force, cutting temperature, tool wear and surface integrity, as presented in Figure 3. Section 4 explores

the emerging trends in UAM, highlighting the transition from a single energy field to dual-field integrated solutions. Section 5 addresses the challenges and presents a future outlook with prospects highlighting new research directions and potential advancement to further improve its application in advanced materials. Finally, the conclusion summarizes the key findings of the research.

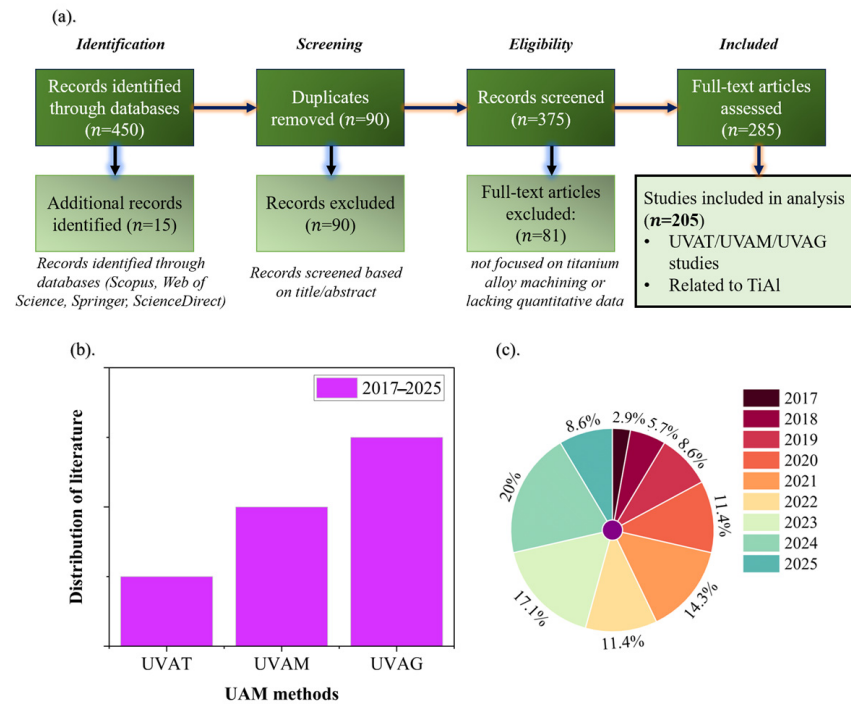


Figure 2. Research trend distribution based on (a) literature selection process (b) machining methods and (c) year.

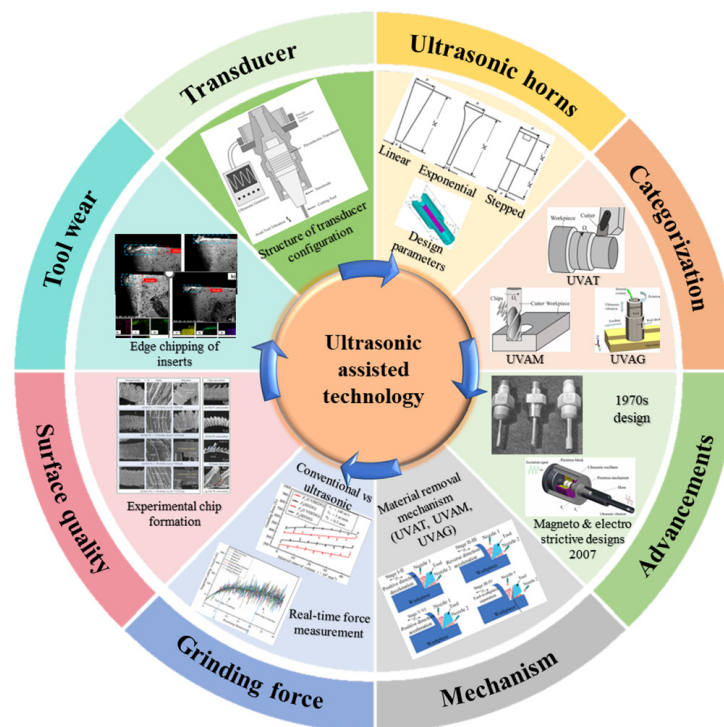


Figure 3. Ultrasonic-assisted machining technology.

2. Characterization and Processing Considerations for Titanium Alloys

2.1. Elemental Composition of Titanium Alloys

The simplest form of Ti–Al alloys is the binary system, consisting of varying proportions of titanium (Ti) and aluminum (Al). These alloys are classified into two major categories, i.e., the alpha (α –TiAl) [15] and gamma phase (γ –TiAl). At lower aluminum content (typically below 10%), the alloy remains primarily in the α -phase, which has a hexagonal close-packed structure [16]. This phase is more ductile and has good formability but does not possess the high-temperature strength that Ti–Al alloys are known for. At higher aluminum content (typically above 40%), the alloy forms the γ -phase, which has a face-centered cubic structure. This phase is more brittle but offers excellent high-temperature strength, oxidation resistance [17] and creep resistance. The γ -phase, specifically Ti–48Al–2Nb, is a popular γ –TiAl alloy, used in high-performance applications. One key challenge in binary Ti–Al alloys is balancing the ductility and toughness of the α -phase with the high-temperature strength and oxidation resistance of the γ -phase. The alloy tends to be brittle due to the γ -phase's properties, requiring a solution to improve its machinability and toughness for practical applications.

The development of γ –TiAl alloys has evolved on the basis of elemental composition through three distinct generations, each improving mechanical properties and high-temperature performance [16,18,19]. The first generation primarily consists of binary compositions with limited ductility and fracture toughness, i.e., Ti–48Al–1V–(0.1 wt.%) C. To enhance the mechanical properties, second generation alloys introduced small alloying elements, i.e., niobium (Nb) [20], molybdenum (Mo) and boron (B) etc., given in Equation (1):

$$Ti - (45 - 48)Al - (1 - 3)X - (2 - 5)Y - (< 1)Z \quad (1)$$

where $X = \text{Cr, Mn, V}$; $Y = \text{Nb, Ta, W, Mo}$; $Z = \text{Si, B, C}$.

The third generation further refined the composition for application-based manufacturability, based on the formula given in Equation (2):

$$Ti - (42 - 48)Al - (0 - 10)X - (0 - 3)Y - (0 - 1)Z - (0 - 0.5) R_e \quad (2)$$

where $X = \text{Cr, Mn, Nb, Ta}$; $Y = \text{Mo, Hf, W, Zr}$; $Z = \text{Si, B, C}$; R_e are rare earth elements [21]. Therefore, the generalized formula for the elemental composition of titanium–aluminum intermetallic alloys is given in Equation (3):

$$Ti - (42 - 48)Al - (0 - 10)(\text{alloying element}) \quad (3)$$

2.2. Binary and Tertiary Titanium Alloys

The brittle nature of γ -TiAl alloys affects their machinability and component reliability. In Figure 4, the element composition and mechanical properties of a binary γ -TiAl have been presented [22,23]. The alloy consists of two major elements: titanium and aluminum [24,25]. The material is manufactured through an additive manufacturing process [26]. The elements are distributed throughout the material [27]. In order to understand the fracture morphology of the material, it was tested at 30 °C as shown. This revealed the intrinsic brittleness, which significantly affects its mechanical performance. Furthermore, the compressive strength of the material was determined at a different interlayer temperature (30–500 °C) during additive manufacturing. The vertical and horizontal direction-based compressive strength shows that the ratio decreases significantly at a high temperature of 500 °C. At room temperature, the compressive strength remains the same in both principal directions.

To further understand the behavior of different tertiary TiAl alloys, different compositions of niobium (Nb), carbon (C), tungsten (W) and silicon (Si) were added. The elemental composition analysis of the material is outlined in Figure 5. At room temperature, the α and γ -TiAl phases were identified at 500 nm, which underpins their mechanical behavior in high-temperature applications [28].

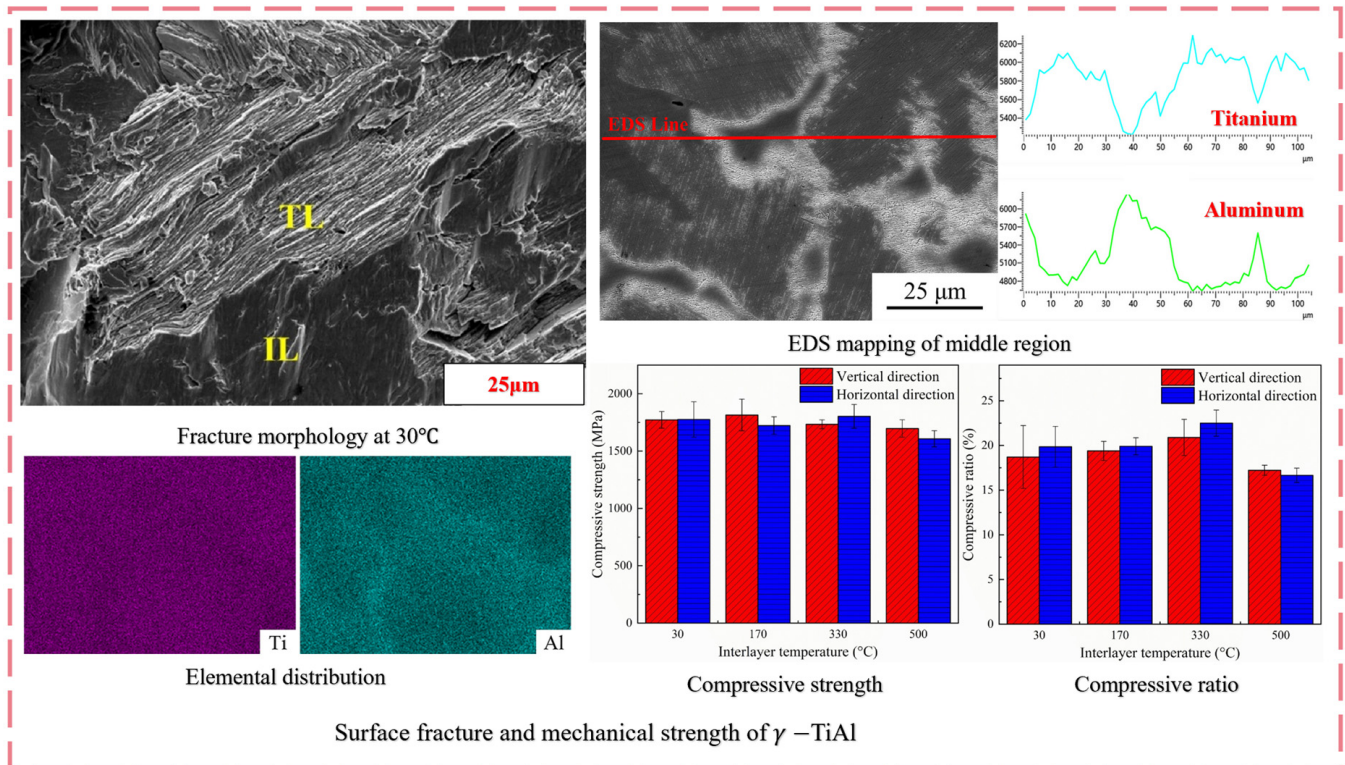


Figure 4. Binary γ -TiAl composition and mechanical strength [22].

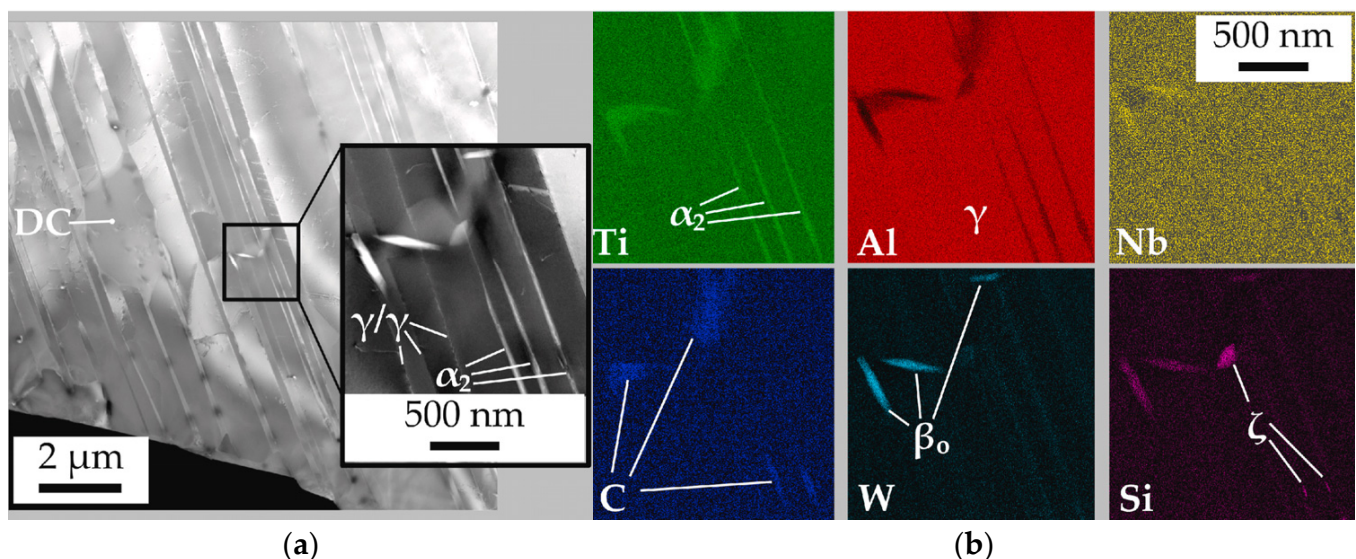


Figure 5. TEM investigations of (a) formation of precipitates and (b) element partitioning [29].

2.3. Properties of Additively Manufactured γ -TiAl Alloy

As discussed earlier, the binary γ -TiAl consists of only two elements resulting in the ordered γ -phase. These alloys exhibit high strength-to-weight ratios at elevated temperatures [30–32]. However, they possess inherent brittle behavior (room ductility ~1–4%)

and limited ductility at room temperature in comparison to tertiary alloys, as presented in Table 1. To introduce certain mechanical and thermal properties, tertiary alloying elements such as Nb, Mo, Cr and Si are added [33]. They affect the properties of the binary aluminides, making them suitable for specific applications. For instance, Nb improves fracture toughness and high-temperature strength, while Mo and Cr enhance creep resistance [33,34]. Si and B refine the microstructure, improving grain boundary strengthening and oxidation. The evolution of binary and tertiary TiAl alloys represents a significant advancement in material science, enabling broader industrial applications with improved performance, durability and manufacturability [35]. However, challenges such as cost-effective processing techniques and maintaining a balance between ductility and strength remain critical research areas for future development [36].

Table 1. Mechanical and thermal properties of binary and tertiary TiAl alloys [37].

Performance	γ -TiAl	Ti ₂ AlNb	α_2 -Ti ₃ Al	TC4
Density ($\text{g}\cdot\text{cm}^{-3}$)	3.7–3.9	5–5.8	4.1–4.7	4.54
Elastic modulus (GPa)	160–180	102–134	110–145	96–110
Yield strength (MPa)	400–800	1030–1292	700–1150	380–1150
Tensile strength (MPa)	450–900	1245–1413	750–1200	480–1200
Room temperature ductility (%)	1–4	3.5–10	2–10	5–20
Thermal conductivity ($\text{W}\cdot(\text{m}\cdot\text{K})^{-1}$)	22–24	7.87	7	6.8–7.95

2.4. Challenges in Additively Manufactured γ -TiAl Alloys

Machining additively manufactured γ -TiAl alloys presents significant challenges due to their inherent brittleness, complex microstructure and high hardness variations [38–41]. Many studies have indicated that the different manufacturing methods obtained by selective elemental composition directly affect the surface friction properties [42–45]. Aspinwall et al. [46] studied the γ -TiAl alloy machining under turning and drilling, but it still poses a challenge. In Figure 6a, the surface often shows workpiece smearing, arc-shaped cracks, subsurface damage and high strain hardening. However, UAM can help reduce these issues. Furthermore, Liu et al. [47] studied the strain rates of forged Ti-46Al-5Nb-1.8Cr-0.2Ta-0.1B alloy to explore the damage evolution at elevated temperatures. For this purpose, mechanical tests at 0.001 to 0.1 s^{-1} strain rates were conducted. In Figure 6b, the strain rate hardening effect on its brittleness has been explained in terms of three modes of fracture. Similarly, Zhang et al. [48] also studied the damage propagation under different temperatures. At room temperature, deformation occurs mainly in γ -lamellae. In Figure 6c, the grain boundaries and phase deformation in tensile testing are presented. Due to tensile loading, the crack initiation at high temperature across grain orientation shows damage behavior. Zhang et al. [49] investigated the surface damage mechanism during nanometric cutting of γ -TiAl. The molecular dynamics simulation method was investigated to determine the influence of cutting parameters and pore defect radii on cutting forces, dislocations and stress, etc. The study is limited by its use of single-crystal models and the need for further exploration of multi-scale defects in real-world conditions as performed by Sahto et al. [50]. It was concluded that the brittle to ductile transition is influenced by the plastic deformation and crack propagation. While these findings are useful for optimizing processing parameters, further research is needed to refine the fracture mechanisms and improve surface quality during manufacturing.

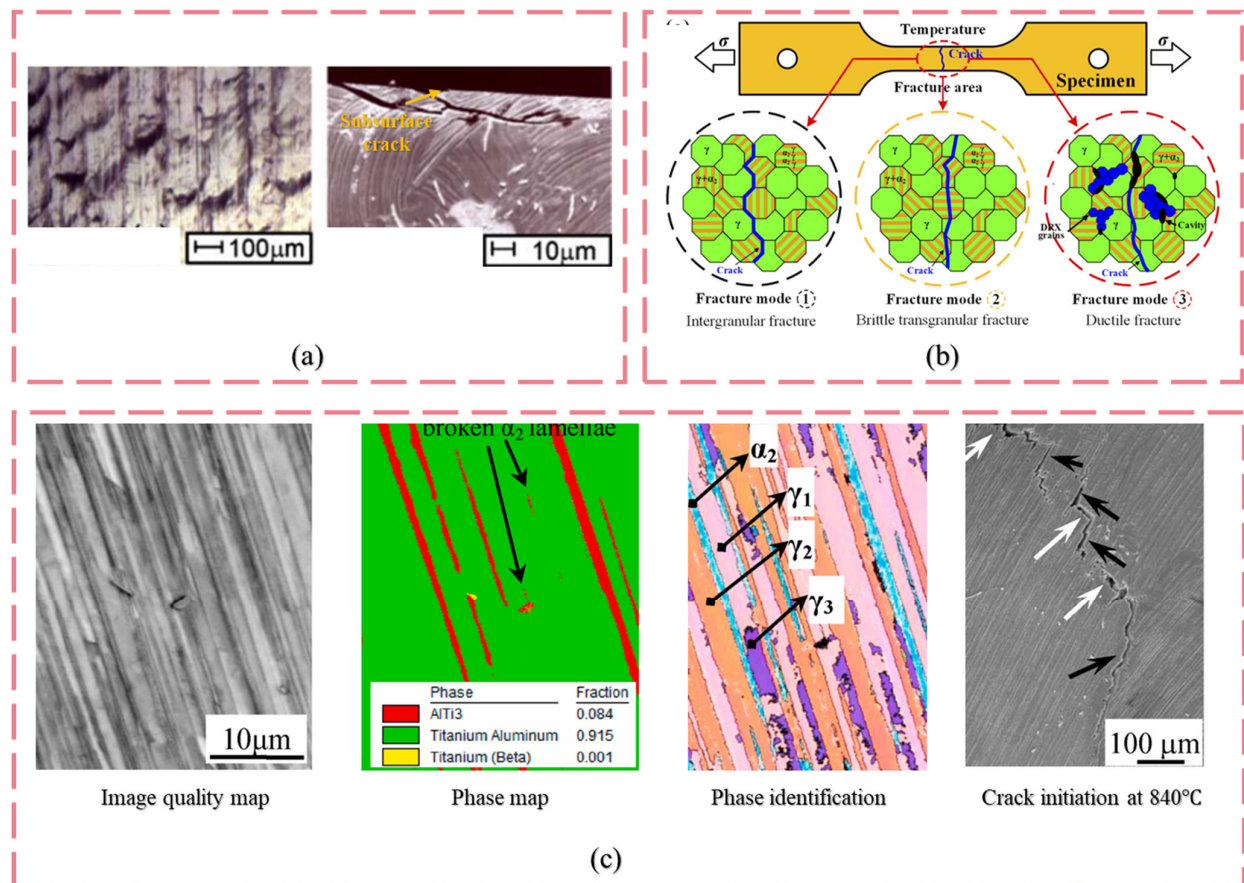


Figure 6. Complex fracture behavior of γ -TiAl based on (a) surface and subsurface damage [46], (b) modes of fracture at micro-scale [47] and (c) EBSD observations under tensile fracture of γ -TiAl [48].

3. Machining Efficiency of Titanium Alloys

The machining efficiency of titanium alloys can be evaluated from the perspective of applied techniques, underlying mechanisms and resulting output parameters [51–55]. Nowadays, advanced techniques, i.e., UVAT, UVAM and UVAG [56], have been widely adopted to improve its machinability [57–60]. These techniques utilize high-frequency vibrations to induce a periodic tool–workpiece separation motion, which reduces the continuous contact between them. The output techniques of UAM are reflected in key performance indicators, i.e., reduced cutting force, lower tool wear rate, improved surface integrity [61] and enhanced dimensional accuracy, having a complex relationship.

3.1. Ultrasonic Vibration-Assisted Turning (UVAT)

The UVAT technique offers distinct benefits depending on the material being machined, the desired output quality and the application requirements [62–64]. This technique applies high-frequency vibrations to the tool during the turning process. It has been divided into sub-categories based on key factors like vibration type, application and performance [65]. The UVAT mechanisms are normally based on the direction of vibration amplitude. It plays a decisive role in machining performance. In axial ultrasonic vibration-assisted turning (AUVAT), the amplitude is aligned axially with the cutting direction, producing an intermittent tool–workpiece separation. On the contrary, rotary ultrasonic vibration-assisted turning (RUVAT) applies amplitude radially, improving chip fragmentation and stability by altering lateral cutting dynamics. While torsional ultrasonic vibration-assisted turning (TUVAT) introduces torsional amplitude around the tool axis, increasing tool edge

stresses. Therefore, conventional UVAT amplitude can be in a single or combined direction depending on proper alignment with the cutting mechanics. The mechanisms behind different UVAT configurations explain their varied performance, as presented in Table 2.

Table 2. Comparative analysis of UVAT technology with respect to conventional turning.

Method	Materials	Percentage Reductions							Ref.	Year	
		F_x, F_y, F_z	F_R	S_a	R_a	T_c	VB	σ_R			TL
AUVAT	Ti6Al4V		↓40%							[66]	2020
UVAT	Ti6Al4V					↓16%		↑166%		[67]	2021
UVAT	Ti6Al4V				↓18.5%		↓70%			[68]	2022
UVAT	Ti6Al4V				↓57%					[69]	2020
AUVAT	Ti6Al4V		↓50%			↓15%			↑102%	[70]	2020
UVAT	Ti6Al4V								↑12%	[71]	2022
RUVAT	Ti6Al4V				↓47%		↓33%			[72]	2018
UVAT	Ti6Al4V			↓43.5%	↓49%					[73]	2014
AUVAT	Ti6Al4V				↓14.2%		↓25%	↑22.5%		[74]	2023
RUVAT	Ti6Al4V	↓51.1%/↓68.3%				↓9.4%				[75]	2021
TUVAT	Ti6Al4V	↓13%/↓21.3%								[76]	2021
UVAT	Ti6Al4V	↓30%/↓70%			↓30%					[77]	2020

Note: ↑ = Increase in value and ↓ = decrease in value.

The comparative analysis of different types of UVAT techniques and their benefits to the machining of TiAl alloy has been presented. AUVAT consistently achieves substantial reductions in cutting forces with reported values ranging from 40% to 50% [66,70], additional benefits in tool life improvement (↑102%) and reduced surface roughness (↓15%). Similarly, RUVAT also demonstrates strong performance, with cutting force reductions of up to 68.3% and notable improvements in tool wear (↓33%) [72,75]. This demonstrates its effectiveness in stabilizing chip formation. Lastly, torsional UVAT (TUVAT) offers moderate reductions in cutting forces (13–21.3%) [76] but stands out for enhancing surface integrity through multi-directional tool motion. Conventional UVAT, while generally effective, shows a broader range of outcomes with cutting force reductions between 16% and 70% [67–69,73,77]. These variations suggest that AUVAT is most suitable for tool wear suppression and productivity gains while RUVAT is most suitable for balanced improvements in force and tool wear. Overall, the vibration mode and its alignment with the tool–workpiece contact mechanics are key determinants of machining performance.

3.1.1. Influence of UVAT on Cutting Force

Cutting force is a key indicator of machining stability. During the turning operation, high cutting forces can lead to rapid tool wear, poor surface quality and increased costs [78]. To address this, researchers have explored UVAT, which enhances the machining performance. Qiu et al. [79] studied the material removal mechanism of Ti-47.5Al-2.5V-1.0Cr alloy during cryogenic machining. The methodology involved turning tests under different cooling media, focusing on the effect of liquid nitrogen cooling on chip formation and material behavior. The results show that cryogenic cooling enhances the brittleness, leading to a change in the material removal mechanism, where periodic brittle fracture occurs near the chip-free surface and ductile-brittle fracture near the cutting edge. As cutting speed increases, the alloy exhibits a sawtooth chip morphology under cryogenic conditions [80,81]. However, the main drawback of high-speed cryogenic machining is the potential for reduced tool life, limiting the feasibility of extremely high cutting speeds in TiAl alloy machining.

It is well known that UVAT technology arises from the periodic separation between the tool and workpiece due to ultrasonic vibrations. Therefore, its effectiveness is largely influenced by the machining parameters, i.e., feed rate, spindle speed and phase shift. In Figure 7, the mechanism of the UVAT system is shown [70]. In the case of conventional turning, the ultrasonic amplitude is zero. The workpiece is allowed to rotate along its axis. The tool cutting action is perpendicular to the workpiece axis. Due to no movement in this direction, the tool continuously remains in contact with the machined surface. This either results in a heat-concentrated region, tool wear or material adhesion. This creates a challenge that needs to be addressed. During UVAT, the ultrasonic vibration is given to the cutting tool in the axial direction of the workpiece. Due to this movement, a separation state results at the cutting interface. This allows the lubrication to assist in reducing the temperature of the tool contact region. This causes a reduction in cutting forces.

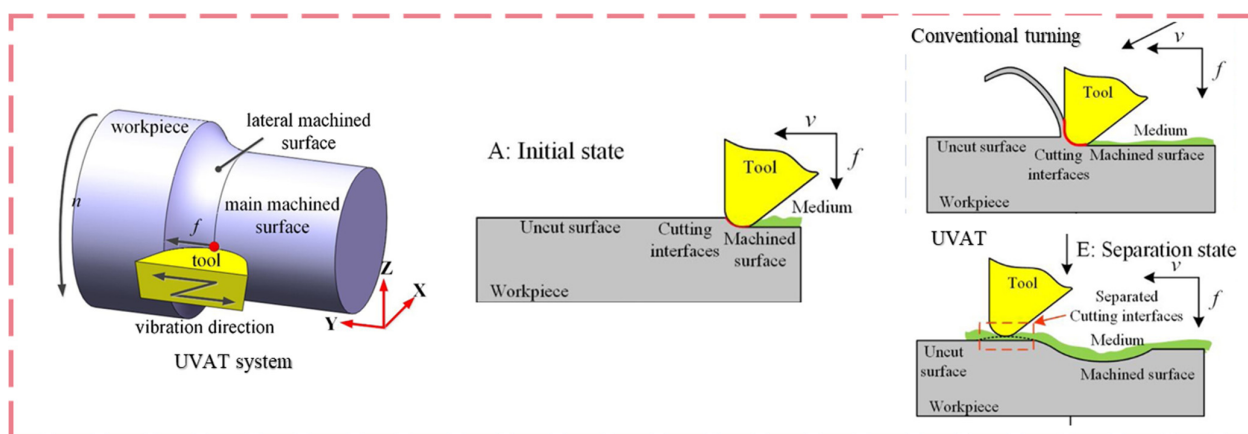


Figure 7. Comparison of conventional and UVAT mechanism [70].

According to the performance characteristics of titanium alloys, researchers have used UVAT for improving the machining process. The comparison of measured forces due to conventional and UVAT studied by Li et al. [82] highlights the reduction in cutting forces across both feed rate and cutting speed. It was also observed that the increase in speed has caused the rise in cutting forces for both conventional and UVAT processes. Chen et al. [75] investigated the effect of UVAT on the machining of Ti6Al4V. Using the finite element method (FEM), a model was developed to analyze the plowing force and its influence on tool wear and surface quality. The cutting forces in the plowing area are evaluated under varying conditions. The results show that UVAT significantly reduces plowing forces compared to conventional cutting with reductions of 13.4–51.1% in F_x and 5.3–68.3% in F_y . Increasing the vibration amplitude further reduces these forces, improving machining efficiency. Overall, UVAT minimizes cutting forces, reducing tool wear, making it a promising technique for Ti6Al4V. Airao et al. [83] analyzed the effect of UVAT of Ti6Al4V under sustainable machining conditions using a vegetable oil based cutting fluid. The comparison between conventional and UVAT under dry and oil-based conditions was conducted to evaluate the surface integrity. The findings reveal that UVAT significantly reduces cutting forces, with an average reduction of approximately 30–45%. The lowest forces were observed under vegetable oil conditions, where cutting forces were reduced by up to 50% compared to dry UVAT. In addition to this, Kandi et al. [84] also examined the impact of UVAT on cutting forces for Ti6Al4V. A horn-based tool holder was designed and FEM was conducted to assess its suitability. A comparison between conventional machining and UVAT was carried out. A significant reduction in cutting forces, achieving 40% lower at 18 m/min, 35% at 30 m/min and 25% at 40 m/min compared to the conventional method. These findings support the idea that UVAT reduces cutting forces. Pei et al.'s [85] study

also explores the influence of UVAT with a major focus on improving surface integrity and reducing tool wear. A series of experiments were conducted. The findings indicate that vibration amplitude is effective for optimizing the machinability of TiAl alloys.

3.1.2. Influence of UVAT on Cutting Temperature

Cutting temperature is important in UVAT technique due to its effectiveness in reducing thermal load, improving tool life and enhancing surface quality. Zhang et al. [86] explores the effect of high-frequency vibrations on cutting temperature in the machining of Ti6Al4V using FEM. Conventional and ultrasonic vibration cutting were simulated in ABAQUS/Explicit using the arbitrary Lagrange Eulerian approach, with cutting speed (40–60 m/min), feed rate (0.08–0.16 mm/rev) and depth-of-cut (0.1–0.5 mm) varied in single-factor tests. The results show that UVAT significantly reduces cutting temperature due to intermittent contact, which allows heat dissipation. The temperature in the UVAT technique fluctuates in a pulse-wave pattern, reaching its peak when the tool fully engages the workpiece and decreasing when the tool detaches. In Figure 8, the effect of cutting parameters on contact temperature has been presented. Sui et al. [87] addressed the thermal challenge in both conventional machining and UVAT. A theoretical model was also developed for comparative analysis. The results show that UVAT reduces cutting temperature. The increase in cutting speed reduces the temperature which is nearly consistent. However, at lower depths and feed rates, the decrease in temperature is high as compared to higher depths and feed rates.

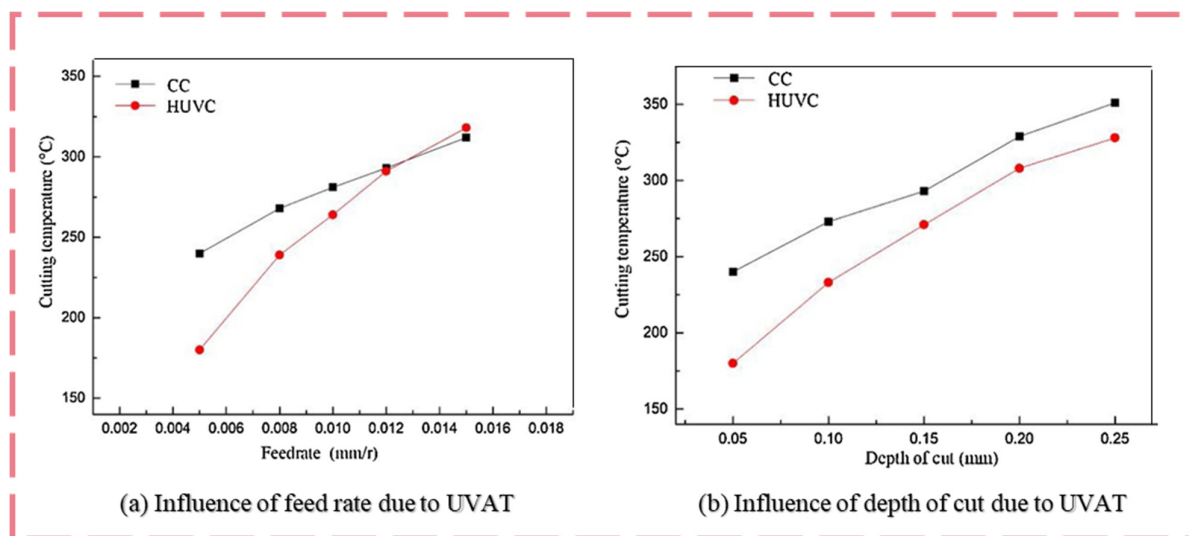


Figure 8. Temperature reduction due to UVAT (a) with depth of 0.05 mm and cutting speed of 200 m/min and (b) feed rate of 0.005 mm/r and cutting speed of 200 m/min, with coolant [70].

3.1.3. Influence of UVAT on Tool Wear

Studies comparing conventional machining and UVAT have demonstrated that tool wear is significantly reduced when high-frequency vibrations are applied. The UVAT process is influenced by several tool wear types, i.e., flank wear, crater wear, built-up-edge (BUE), chipping fracture and adhesion wear. In Figure 9, Airao et al. [68] observed tool wear and tool life in the machining of Ti6Al4V using conventional and UVAT under dry, wet, minimum quantity lubrication (MQL) and liquid carbon dioxide (LCO₂). The results showed that LCO₂ combined with UVAT significantly reduces tool wear. It assists in eliminating the BUE, minimizing flank and crater wear due to its superior cooling effects. Compared to dry conditions, the average width of flank wear reduced by 35%, 54% and 70% under wet MQL and LCO₂ conditions, respectively. The reduction in crater wear was also

observed across all cooling strategies. As a result, tool life was extended significantly, and the machining process became more sustainable. Yan et al. [72] also studied the combined effect of LCO₂ with UVAT. The findings also highlight its superiority in improving tool longevity for TiAl alloys. Sivareddy et al. [88] also examined tool wear and tool life using an uncoated carbide cutting tool at varying cutting speeds (90–150 m/min) and ultrasonic power levels (80–100%). Tool and flank wear were analyzed using a scanning electron microscope (SEM). Tool life improvement in UVAT was highest at maximum ultrasonic power (100%) and lower cutting speeds with enhancements of 62%, 53.2% and 32% at 90, 120 and 150 m/min, respectively. Similarly, increasing ultrasonic power at a fixed cutting speed of 90 m/min extended tool life by 18%, 55% and 62% for 80%, 90% and 100% power levels. This concludes the benefits of using high-frequency vibrations.

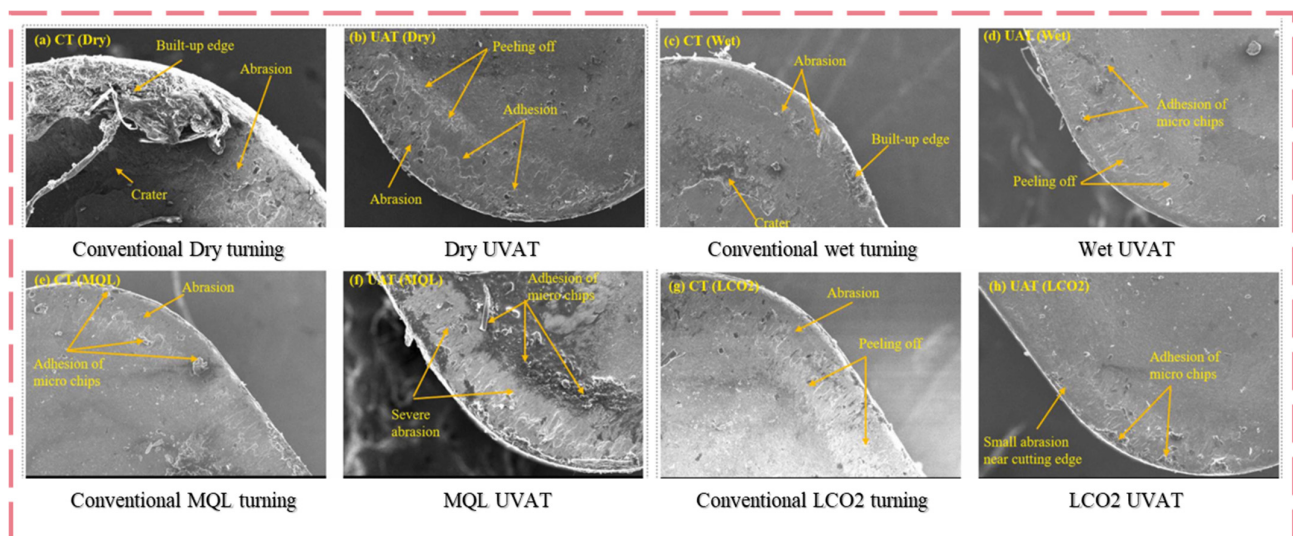


Figure 9. Comparison of crater wear conventional turning under (a) dry (c) wet (e) MQL and (g) LCO₂ conditions and UVAT under (b) dry (d) wet (f) MQL and (h) LCO₂ [68] conditions.

3.1.4. Influence of UVAT on Surface Integrity

Surface integrity is a critical factor in the performance of longevity of TiAl components [89]. Yan et al. [72] conducted a study to show the impact of conventional turning and UVAT under dry and MQL conditions. Under dry machining conditions, a higher surface roughness is observed due to increased adhesion and friction at the chip–tool interface. This also resulted in severe groove and notch wear. The study concluded that UVAT and MQL combined provide the best surface finish, demonstrating their effectiveness in improving the processing of this material. A study by Silberschmidt et al. [73] discussed the effect of UVAT on surface roughness across a broad range of metals and alloys, including copper, aluminum, stainless steel and titanium alloys. However, the degree of improvement varies depending on the specific material and machining parameters. Overall, the study validates that UVAT is an effective technique for difficult-to-cut materials.

Although UVAT improves the surface quality of the machined surface, it also results in the formation of micro-structures. The micro-structures are dependent on the vibration amplitude along the longitudinal and transverse direction of the tool movement. According to Lofti et al. [77], the 3-dimensional elliptical ultrasonic vibration-assisted turning (EUAT) results in surface microstructural change, including surface roughness, micro-hardness and surface isotropy. Experimental and 3D-finite element simulations were conducted to investigate these effects under different cutting conditions. The results showed that elliptical UVAT significantly reduced grain size, leading to improved surface hardness. The technique also produced semi-spherical micro-textures that enhanced surface isotropy,

providing a more uniform surface compared to conventional turning, as shown in Figure 10. Surface roughness R_a (μm) was also found to be lower than conventional processing. The method effectively controlled excessive variations in roughness by stabilizing cutting forces. Overall, the use of high-frequency vibrations in the turning process for titanium alloys improves surface uniformity while maintaining appropriate surface roughness.

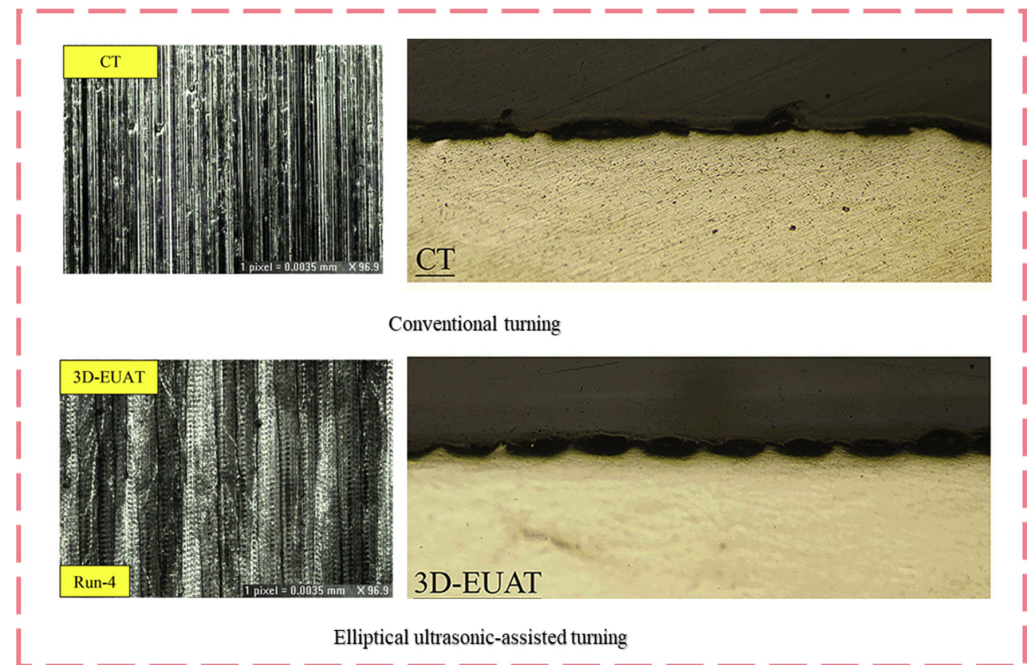


Figure 10. Surface morphology due to conventional and elliptical UVAT at feed rate 0.11 mm/rev, speed 15 m/min and depth of cut 0.5 mm [77].

3.2. Ultrasonic Vibration-Assisted Milling (UVAM)

UAM offers significant advantages over traditional machining by incorporating high-frequency vibrations into the tool's motion. When this technology is combined with the milling process, the need for a high material removal rate (MRR) can be achieved. The integration of high-frequency in the milling process is termed ultrasonic vibration-assisted milling (UVAM) [90,91]. This process is dependent on the tool relative displacement generated with respect to the workpiece [92,93]. This is a key distinguished feature of this method, which is significantly different from conventional milling, as demonstrated in Table 3. Sun et al. [94] discussed the conventional tool-tip trajectory by superimposing high-frequency oscillations onto the cutting motion. It was found that this mechanism is influenced by the amplitude and frequency. Gu et al.'s [95] review also examines the intermittent separation cutting characteristics under specific machining conditions. It also discusses the effect of tool motion trajectory on surface morphology, chip formation and tool wear. The findings emphasize that further investigation into the tool's motion trajectory can potentially address existing challenges in UAM, paving the way for more efficient and precise machining solutions.

In Table 4, the summary related to the processing of titanium alloys by the use of UVAM has been presented. The literature related to it uses longitudinal vibration (L-UVAM), feed direction (FD-UVAM) and longitudinal torsional ultrasonic vibration-assisted milling (LT-UVAM) [96]. In L-UVAM, the ultrasonic vibrations are applied in the axial direction of the tool (parallel to the spindle). This results in the tool moving up and down along its axis during milling [97]. The key advantages include improved cutting efficiency, reduced cutting forces and enhanced chip evacuation due to intermittent tool–workpiece contact [98–100]. In the FD-UVAM approach, the ultrasonic vibration is

applied in the direction of the tool feed. The periodic acceleration and deceleration in the feed direction led to better chip segmentation and reduced adhesion at the tool–workpiece interface. Lastly, the LT-UVAM approach is a hybrid technique that combines longitudinal and torsional vibration. This results in a more complex motion where both axial and rotational oscillations contribute to the cutting action. The combined effect of these vibrations minimizes the cutting resistance.

Table 3. Tool motion trajectory in various UVAM methods.

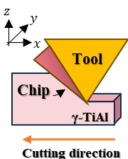
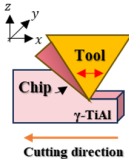
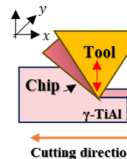
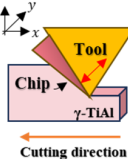
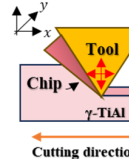
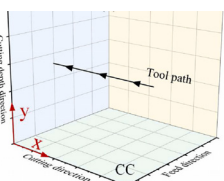
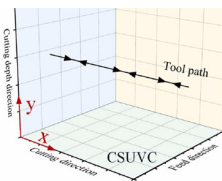
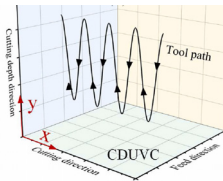
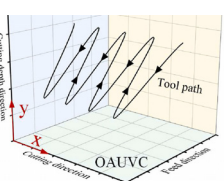
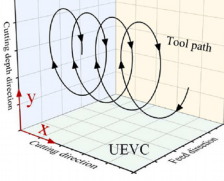
Without Vibration	Vibration in Cutting Direction	Vibration to Normal to Surface	Vibration Normal to Cutting Direction	Compound Vibration
 $x(t) = v_c t$ $z(t) = 0$	 $x(t) = v_c t + A_x \cos(2\pi f t)$ $y(t) = 0$ $z(t) = 0$	 <p>Tool trajectory equations</p> $x(t) = v_c t$ $y(t) = A_y \cos(2\pi f t)$ $z(t) = 0$	 $x(t) = v_c t$ $y(t) = 0$ $z(t) = A_z \sin(2\pi f t)$	 $x(t) = v_c t + A_x \cos(2\pi f t)$ $y(t) = A_y \cos(2\pi f t + \phi_1)$ $z(t) = A_z \sin(2\pi f t + \phi_1)$
Trajectory plots				
				

Table 4. Comparative analysis of UVAM technology with respect to conventional milling.

Method	Materials	Percentage Reductions								Ref.	Year
		F_x, F_y, F_z	F_R	S_a	R_a	T_c	VB	σ_R	TL		
LUVAM	TC18	-	↓34.1%	↑85%	-	↓19.5%	-	↑50%	-	[101]	2022
FDUVAM	Ti6Al4V	-	-	-	↓30%	-	-	-	-	[102]	2019
LTUAM	Ti6Al4V	↓29.1% /↓34.7%	-	-	-	-	↓18%	-	-	[103]	2021
UVAM	TC18	-	↓16.1%	-	↓45.7	-	-	-	-	[104]	2022
LBUAM	TC4	↓32.3%/31% /6.6%	-	↓35%	-	-	-	-	↑166%	[105]	2022
LTUAM	Ti6Al4V	-	↓40%	↓74.6%	-	-	-	-	-	[106]	2018
LTUAM	Ti6Al4V	↓36%	-	-	-	↓25%	-	↑25%	-	[107]	2020
LUVAM	Ti6Al4V	-	↓55%	-	↓15%	↓17%	-	-	-	[108]	2020
LUVAM	Ti6Al4V	-	-	-	↓24%	-	-	-	-	[109]	2022
LTUAM	Ti6Al4V	-	↓14%	-	-	-	↓30%	-	-	[110]	2020
LUVAM	Ti6Al4V	-	-	-	-	-	↓67%	↓26%	-	[111]	2018
UVAM	Ti6Al4V	-	↓56.5%	-	-	-	-	-	-	[112]	2022
LUVAM	Ti6Al4V	-	↓12.2%	-	↑27.9%	-	-	-	-	[113]	2022
LUVAM	Ti6Al4V	-	↓18.6%	-	↓24%	↓15%	-	-	-	[114]	2023
LUVAM	TC18	-	↓15.6%	-	↓44%	↓42%	-	↑40%	-	[115]	2023
LUVAM	Ti6Al4V	↓15%	-	-	↓72%	-	-	-	-	[116]	2023
LTUAM	Ti6Al4V	↓45.1%	↓28.9%	-	-	-	-	-	-	[117]	2022
LUVAM	Ti6Al4V	↓14.6%/- /↓30.2%	-	-	↓35.1%	↓25.9%	-	-	-	[118]	2022

Note: ↑ = Increase in value and ↓ = decrease in value.

3.2.1. Influence of UVAM on Cutting Force

The analysis of cutting force in UVAM is conducted by calculating tool trajectory, instantaneous chip thickness and tool vibration magnitude [92]. Ming et al. [119] conducted an experimental and theoretical study for Ti6Al4V processing. The study focused on analyzing the reduction in cutting forces by evaluating tool trajectory. Experimental results demonstrated that UVAM significantly reduced tangential and radial plowing force coefficients by 32.16% and 42.77%, respectively. Overall, the study demonstrates that UVAM effectively decreases cutting forces in tangential and radial directions, although axial forces require further optimization for an enhanced process stability. Similarly, Gao et al. [103] examined the relationship between tool flank wear and cutting forces in UAM of Ti6Al4V under dry conditions, comparing it with conventional milling. In Figure 11a, the measurement of cutting forces using an oblique cutting model is presented. This model uses cutting force coefficients that were calibrated through mechanical methods and time-frequency transformation to analyze the force behavior. Experimental results validated the model, showing an average error of 19.1% and 12.9% for F_x and F_y , respectively. Compared to conventional machining, the cutting forces were reduced, with F_x decreasing by 7.4% to 29.1% and F_y by 34.7% to 40.1%. The presence of a high frequency signal (33.1 kHz) confirmed the impact of ultrasonic vibration, demonstrating the method's effectiveness. In Figure 11b, the benefit of UVAM was also presented by Niu et al. [114]. In addition to this, Rinck et al.'s [120] study focused on developing an analytical force model for predicting cutting forces in UVAM, addressing the challenge in machining Ti6Al4V. The model considers both intermittent and non-intermittent cutting conditions by considering the relative contact ratio between the rake face and chip for shearing calculations. Implemented in MATLAB, the model predicts cutting forces without requiring experimental data. The predicted forces align well with experimental results, demonstrating the model's accuracy. Future research can expand its application to different workpiece materials and tool geometries, enhancing its versatility in cutting force prediction.

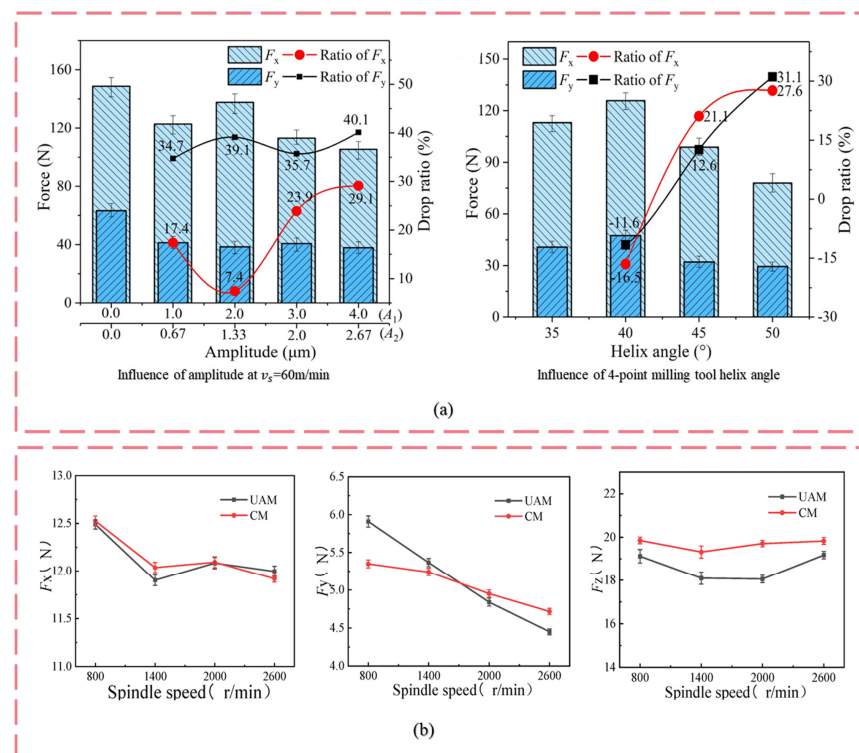


Figure 11. Cutting force (a). conventional milling and UVAM on F_x and F_y [103] and (b) effect of spindle speed (feed = 0.01 mm/z, depth of cut = 0.2 mm and amplitude 3 μm) on F_x , F_y and F_z [116].

Advanced force models and vibration-assisted milling techniques have significantly reduced cutting forces. However, further research is needed to refine predictive models by incorporating more complex tool geometries, varying workpiece materials and dynamic process conditions. Future studies should also explore real-time force monitoring, adaptive strategies and the integration of intelligence tools to enhance precision machining [121].

3.2.2. Influence of UVAM on Cutting Temperature

The superimposition of high-frequency vibrations alters the heat generation and dissipation mechanisms compared to conventional machining. In conventional machining, cutting heat is generated by plastic deformation in the shear zone [122,123]. This is due to the friction between the tool and chip as well as with the workpiece. The intermittent tool–workpiece contact in UVAM influences the heat distribution. As a result, UVAM is beneficial in machining temperature-sensitive materials, i.e., titanium and superalloys.

Cutting temperature at the tool tip directly affects the tool life in titanium alloy processing. In another study [108], the comparison of tool wear between conventional milling and UVAM shows that it reduces the contact temperature as well as improves tool life. According to Niu et al. [114], the effect of cutting speed on temperature evolution is shown in Figure 12. At a low speed, UVAM reduces the maximum cutting temperature. As the speed increases, this difference diminishes. Feng et al. [124] studied the temperature distribution and phase transformations based on simulation. The results indicate that the average temperature distribution is higher in extrusion rather than in shearing with respect to cutting distance.

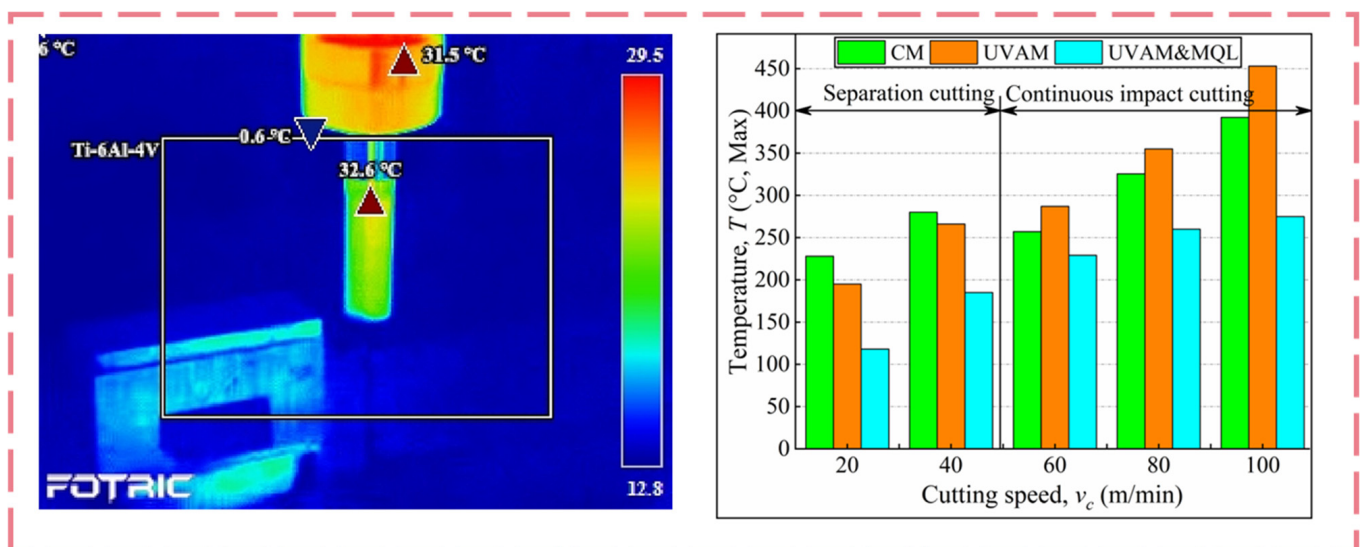


Figure 12. Real-time infrared image and cutting temperature T_c (°C) variation (ultrasonic amplitude 5 μ m, frequency 32.6 kHz, longitudinal direction) [114].

It is found that the use of high-frequency vibration effectively reduces the cutting temperature. Rauf et al. [125] explored this effect of the reduction in cutting temperatures in UVAM of Ti6Al4V under various cooling conditions. Utilizing a Taguchi L16 orthogonal array, the research systematically examines the effects of cutting speed, feed per tooth, depth-of-cut, cooling conditions and ultrasonic amplitude on cutting temperatures. Key findings revealed that the depth-of-cut significantly influences temperature reduction, followed by feed per tooth and cutting speed. It was also observed that cryogenic cooling demonstrates superior performance in terms of heat dissipation [126–128]. Similarly, Li et al. [129] focused on heat treatment and machinability of the γ -TiAlNb intermetallic compound, which is considered a promising material for aircraft structural components. A

46Ti46Al8Nb alloy was subjected to vacuum heat treatment at temperatures between 950 and 1280 °C, with varying holding times (24 h, 1 h and 0.5 h) followed by furnace cooling. The results show that as-cast material consists of γ -phase with the same amount of α -phase AlTi. Heat treatment causes the phase change but improves the machinability by reducing cutting forces in all directions. However, the study indicates that further optimization is needed to fully address the wear resistance. This indicates that hydrostatic pressure near the tool drives phase transformations, affecting cutting resistance [130]. Overall, the findings provide insight into the cutting force mechanisms at the nanoscale, aiding in the optimization of ductile machining in brittle materials.

3.2.3. Influence of UVAM on Tool Wear

Flank wear is a critical factor in machining efficiency and product quality. In conventional milling, flank wear expands the tool–workpiece contact area, leading to higher temperatures, increased forces and severe tool peeling [131–135]. As depicted in Figure 13a, the LT-UVAM mechanism using an AlTiN-coated carbide tool is presented by Gao et al. [103]. It was observed that high-frequency vibration reduces thermal cycling, minimizing excessive wear and tool failure. Additionally, the axial force (F_z) in LT-UVAM is dynamic due to ultrasonic impact and its increase with helix angle stress concentration. The study concluded that a larger helix angle accelerates tool wear, making it unsuitable for this machining approach. Wang et al. [136] also discussed tool behavior in the milling of γ -TiAl alloy (Ti-47.5Al-2.5V-1.0Cr) under different machining conditions. A full-factorial design (3-factors, 3-levels, 27 tests) was used to examine the impact of process parameters. Figure 13b shows the primary wear mechanism observed on the flank and rake wear. This study confirms that increasing tool wear significantly impacts its degradation. Moreover, Priarone et al. [137] investigated tool wear and tool life in the milling of gamma titanium aluminide (γ -TiAl) fabricated via electron beam melting and subsequent thermal treatment, a material of aeronautic interest known for its challenging machinability. The study concludes that optimizing lubrication strategies, tool geometry and coatings is essential for improving tool life and machinability when milling γ -TiAl. Lastly, Zhang et al. [138] also validated that UVAM helps in extending tool life. Figure 13c shows the initial profile of the tool, which should be coordinated with processing parameters to achieve better performance.

From the previous discussion, it is concluded that UVAM has significant potential in reducing tool wear compared to conventional milling, primarily due to its intermittent cutting nature. However, despite these advantages, a major challenge remains: the increased dynamic loading on the tool due to high-frequency vibrations, which can lead to micro-chipping and fatigue failure over extended machining durations [139–141]. To fully leverage UVAM's benefit, future research should focus on optimizing tool geometries and vibration parameters to mitigate dynamic effects while maintaining efficiency for γ -TiAl.

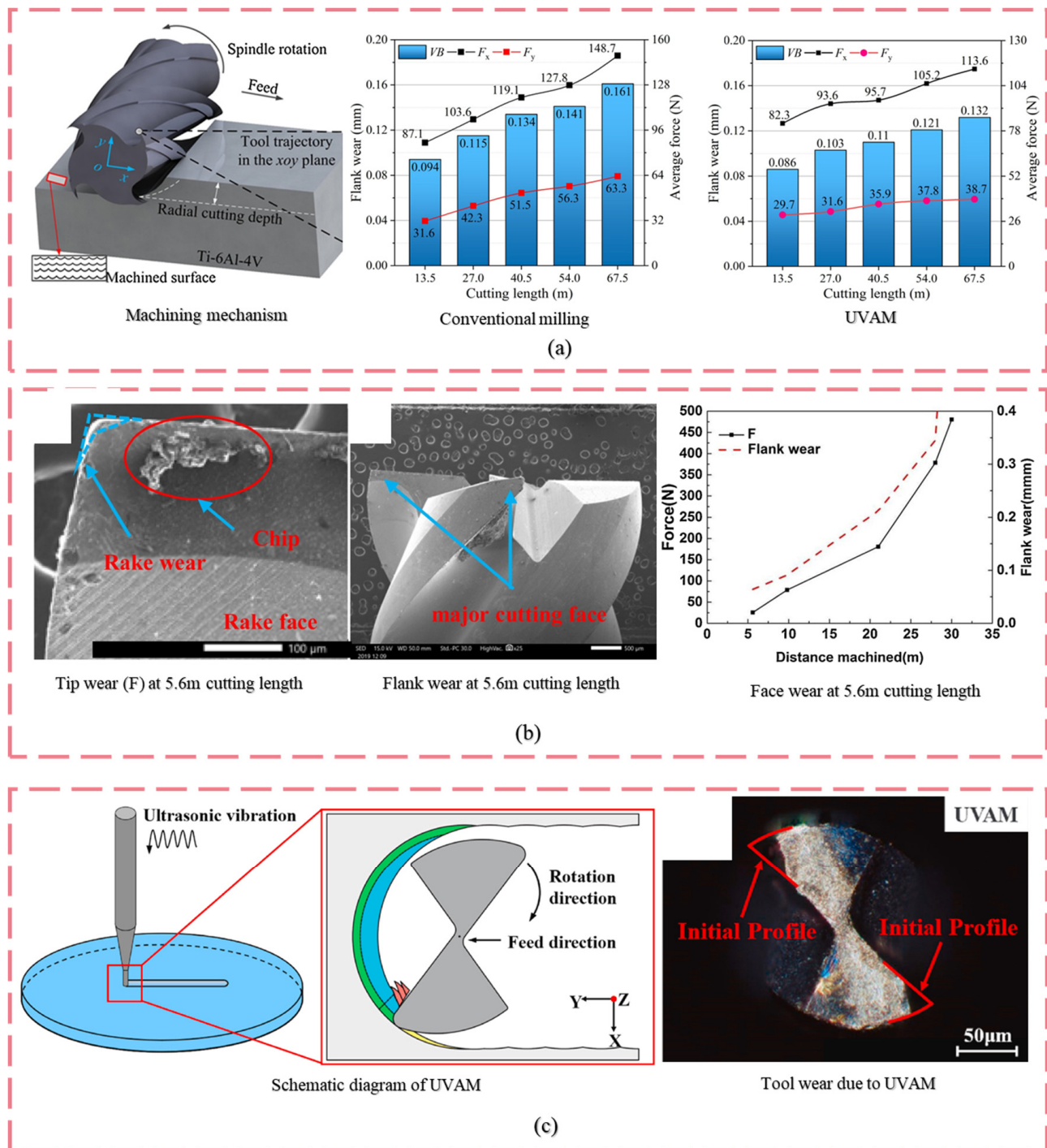


Figure 13. Tool wear (VB) based on (a) influence of flank wear on average cutting force (F_{avg}) during conventional (speed = 60 m/min) and ultrasonic [103] (b) flank and rake wear with cutting length 5.6 m [136] (c) wear pattern in UVAM [138].

3.2.4. Influence of UVAM on Surface Integrity

UVAM influences the microstructural evolution of γ -TiAl alloys, directly impacting surface integrity. The high-frequency vibration superimposed on the cutting motion induces unique deformation mechanisms, including localized grain refinement, work hardening and dynamic recrystallization [142], which enhance the surface properties of the machined TiAl components [143,144]. In addition to this, the oscillatory nature of UVAM imparts micro-textured patterns or periodic surface marks that may appear [129]. This results in affecting the roughness and tribological behavior of the machined surface. In Figure 14a,

the surface morphology under various conditions has been presented to show the effect of high-frequency vibration [114]. In conventional milling, adhered material and plowing phenomenon were observed. However, UVAM results in adhered microparticles and ultrasonic ironing of the surface. This is due to the intermittent contact behavior. Guo et al. [145] conducted a comparative study on subsurface damage between conventional milling and UVAM, as shown in Figure 14b. The UVAM process, with a vibration amplitude of 4 μm introduces fine sinusoidal vibration textures in addition to the conventional tool feed trajectory. In conventional milling, distinct ridged textures appear due to the cutting-edge feed, with noticeable chatter marks at higher feed rates. The results suggest that UVAM alters the surface morphology, potentially impacting functional performance.

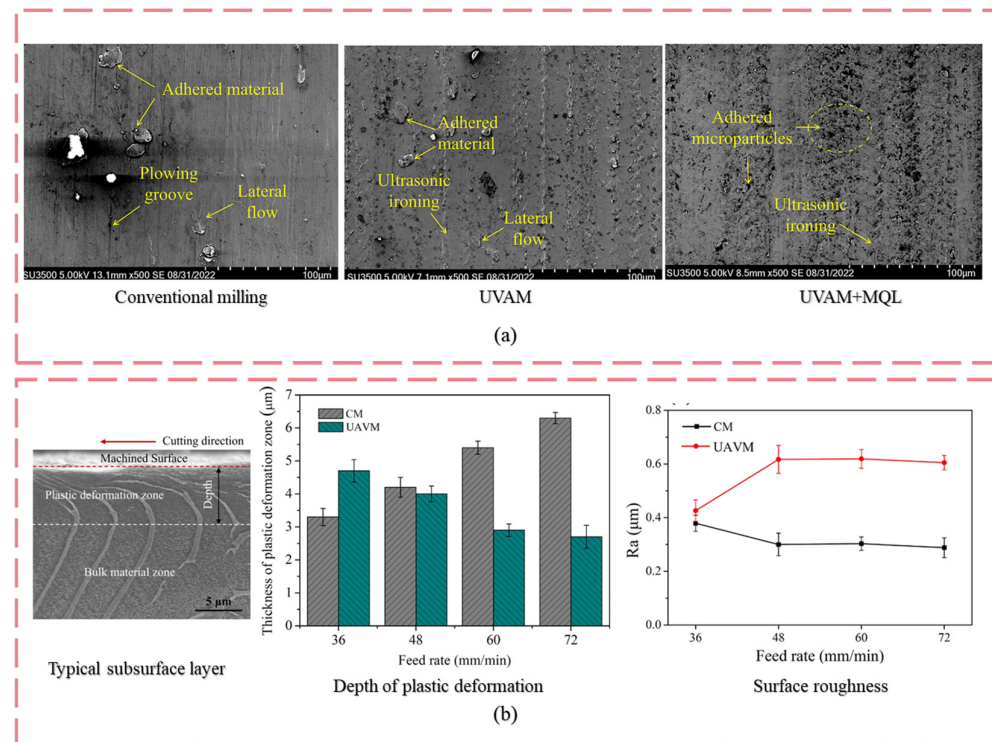


Figure 14. Surface morphology based on (a) comparison of conventional, UVAM and MQL+UVAM machining [114] (b) Subsurface damage and roughness R_a (μm) [145].

3.3. Ultrasonic Vibration-Assisted Grinding (UVAG)

UVAG machining method integrates high-frequency vibrations into conventional grinding processes to enhance the material removal efficiency and surface quality [146]. By applying ultrasonic vibrations, typically in the range of 20–40 kHz [58], the grinding force is significantly reduced, improving tool life and reducing heat generation [147]. This process is particularly effective for hard and brittle materials, such as titanium alloys and ceramics, as it minimizes subsurface damage and improves chip formation mechanisms. The UVAG method can be classified based on tool–workpiece relative motion.

The UVAG method uses a lower depth-of-cut (typically in micrometers) for precision and surface quality. Lower MRR is focused on controlled material removal and surface integrity [148]. In contrast, ultrasonic vibration-assisted high-efficiency deep grinding (UVHEDG) uses a significantly higher depth-of-cut (typically in millimeters) to achieve deep grinding in a single pass [149]. High MRR is due to deeper penetration and aggressive cutting. This method is highly productive for grinding hard materials, i.e., aerospace components and automotive parts. A summary of these methods has been outlined in Table 5.

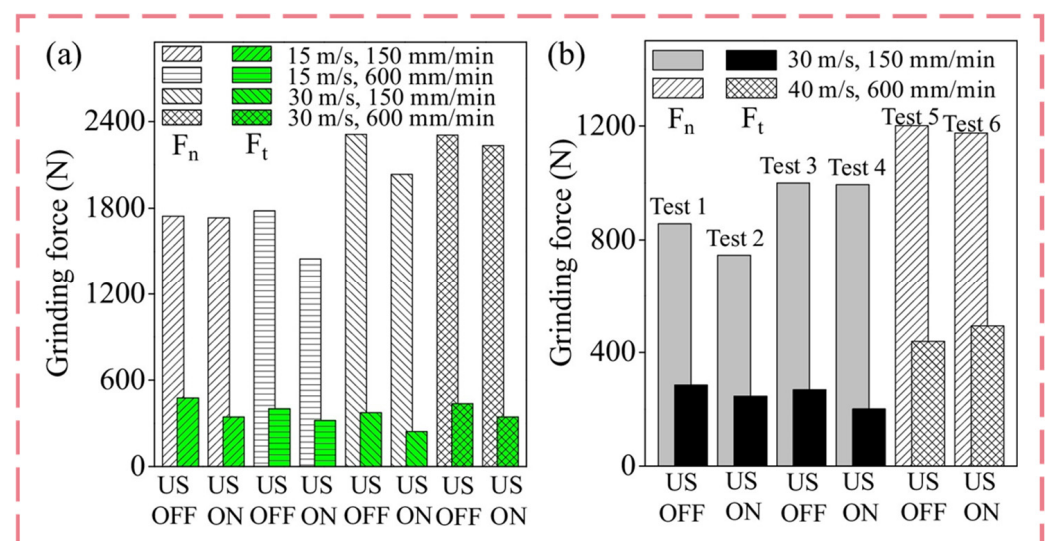
Table 5. Comparative analysis of UVAG with respect to conventional grinding.

Method	Materials	Reductions					Ref.	Year
		F_t/F_n	F_R	R_a	T_c	VB		
UVHEDG	γ -TiAl		↓38.7%	↓19.5%	↓39.1%		[150]	2023
UVAG	γ -TiAl			↓20.1%			[37]	2024
UVHEDG	γ -TiAl				↓39.1%		[151]	2025
UVAG	γ -TiAl	↓35%/↓19%		↓10%			[152]	2017
UVAG	Ti6Al4V	↓35%/↓39%					[153]	2020
UVAG	Ti6Al4V	14.2%/13.5%		↓10%			[154]	2012
UVHEDG	γ -TiAl	16.2%/14.7%		↓46.5%	↓15.4%		[149]	2024
UVAG	γ -TiAl		↓25%	↓45.9%			[155]	2023
UVAG	TC4					↓25.2%	[156]	2022
UVAG	γ -TiAl		↓40.5%		↓38.7%		[157]	2020

Note: ↑ = Increase in value and ↓ = decrease in value.

3.3.1. Influence of UVAG on Cutting Force

In the UVAG method, the periodic separation between the abrasive grains and the workpiece reduces the average normal and tangential forces compared to conventional grinding. This reduction is attributed to the intermittent contact, which minimizes friction and thermal effects, which can be explained through mechanistic models. Li et al. [147] proposed a grinding force prediction model for ultrasonic grinding of γ -TiAl material. The model is based on the chip formation mechanism of abrasive sliding, grinding and high-frequency assisted machining, considering shear effects, plastic deformation and friction. The predictions were compared to the experimental results, in which showed a 23% deviation in tangential force and 21.7% deviation in the normal force, indicating a good agreement between the two. The model can also predict grinding forces for different materials by adjusting parameters, though the deviations suggest room for further refinement, especially in highly variable conditions. Similarly, Li et al. [158] also proposed grinding models for other aerospace materials.

**Figure 15.** Grinding force F_n & F_t with (a). SiC wheel and (b) electroplated diamond wheel [152].

In Figure 15, the UVAG experimental setup and material removal mechanism has been presented by Chen et al. [149]. The ultrasonic vibrations are applied in the feed direction. This allows the lubrication liquid to flow in the grinding arc. Moreover, Song et al. [159] conducted a parametric study to show the relationship between the evolution

of the grinding force. The research shows the grain wear mechanism in UVAG of γ -TiAl material. The results indicate that UVAG enhances material removal efficiency by reducing adhesion and grinding forces due to periodic impact forces. However, when the unformed chip thickness exceeds $0.8\text{ }\mu\text{m}$, grains are more likely to experience macro-fracture, reducing grinding efficiency. At grinding speeds over 80 m/s , increased thermal damage leads to material adhesion, further decreasing effectiveness. Additionally, ultrasonic amplitudes above $6\text{ }\mu\text{m}$ significantly increase impact forces, making boron nitride grains susceptible to cleavage fractures and accelerating wear.

3.3.2. Influence of UVAG on Cutting Temperature

In UVAG, temperature control is a critical factor influencing grinding performance. The application of high-frequency ultrasonic vibrations, which reduces continuous friction between abrasive grains and the workpiece under various lubrication conditions, [160,161] leads to lower average temperatures compared to conventional grinding. However, localized temperature rise can still occur due to periodic impact forces, especially at high vibration amplitudes. The reduction in thermal load enhances tool life and minimizes thermal damage. Chen et al. [149] addresses issues such as burns and tool wear during high-efficiency deep grinding with the aid of ultrasonic vibrations. The results show that high-frequency vibration reduces the grinding temperature by an average of 15.4% when compared with deep grinding. It was also determined that the wear of micro-grain is significantly improved with ultrasonic vibrations. These findings demonstrate that high-frequency vibration results in smoother surface morphology, a shallow plastic deformation layer and shear-like chip shapes due to it. Further studies are needed to fully understand the long-term effects of ultrasonic assisted vibrations on tool wear and material performance [162,163]. Yang et al. [37] investigated the machining performance of γ -TiAl intermetallic compound (Ti-45Al-2Mn-2Nb) through ultrasonic assisted grinding. Gray relational analysis was used to determine the optimal machining parameters with best condition as $F_n = 3.22\text{ N}$, $F_t = 1.08\text{ N}$ and $T = 174\text{ }^\circ\text{C}$. Ultrasonic vibration decreased surface roughness by up to 20.12%, with a maximum profile height of $1.94\text{ }\mu\text{m}$. A potential drawback is that the impact of material microstructure variations and long-term performance under industrial-scale conditions was not fully explored.

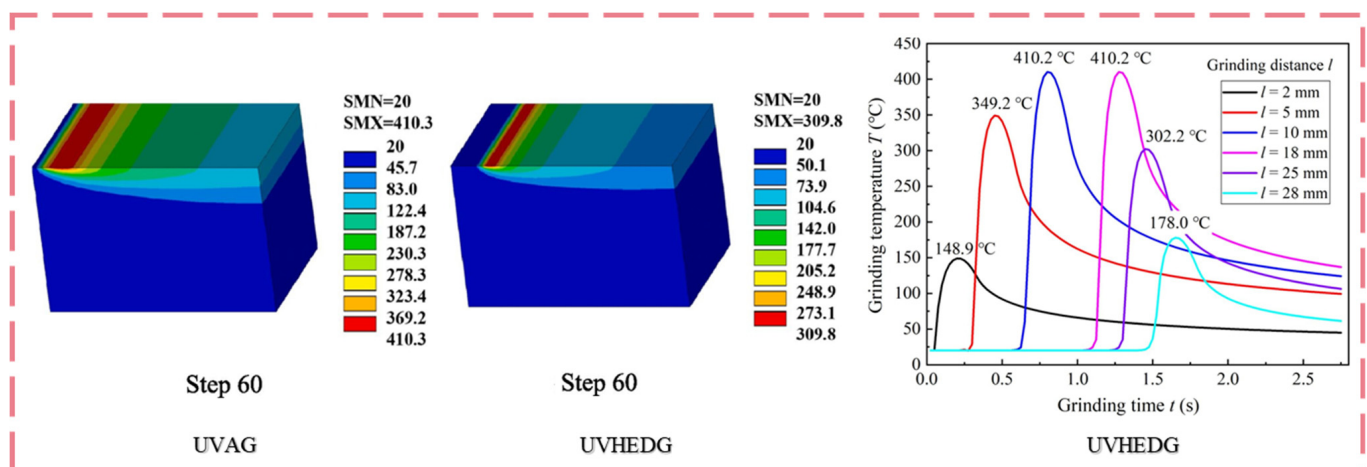


Figure 16. Temperature (T_c) distribution based on simulation results at grinding distance (2–28 mm) [151].

The grinding performance of this material machining using ultrasonic-assisted deep grinding is significant. The key performance indicators include grinding force and temperature, which have been studied by Wang et al. [150], having 38.69% and 39.05% reductions,

compared to high-efficiency grinding. The ultrasonic vibrations enhance the sharpness of the abrasive grains, resulting in 23.95% reduction in specific energy. However, at high-speed grinding, the ultrasonic weakening effect slightly reduces the vibration cycles. In Figure 16, the simulation and experimental outcome of the UVAG of the γ -TiAl blade tenon has been presented. Zhao et al. [151] conducted a simulation with a 3D meshed model using Solid70 hexahedral elements, and accurately captured the temperature evolution across different grinding stages. Results showed that grinding temperature increased rapidly in the initial phase, stabilized during the steady-state grinding, and decreased as the heat source transitioned out. Experimental findings validated the simulation results, with a discrepancy of 2.3% to 13.1%. Compared to HEDG, UVHEDG exhibited 37–38.25% lower temperatures, attributed to the intermittent “contact-separation” cycle that enhanced heat dissipation by allowing better coolant penetration. The highest grinding temperature recorded in HEDG was 877.2 °C, while UVHEDG peaked at 647.1 °C. The linear increase in temperature with grinding speed and workpiece velocity was confirmed, demonstrating that ultrasonic vibration significantly reduces grinding temperature and the heat-affected zone, improving thermal control in machining processes.

3.3.3. Influence of UVAG on Tool Wear

In UVAG, the constant grain trajectory results in prolonged contact time between the abrasive grains and the workpiece, leading to the formation of wear flats. As the shearing forces exceed the grain's bonding strength, abrasive pull-out occurs, accelerating tool wear and degrading machining performance [164]. In contrast, ultrasonic vibration-assisted high-efficiency deep grinding (UVHEDG) minimizes abrasive pull-out by reducing the grain's continuous contact, leading to only microscopic fracturing rather than large-scale grain loss. This helps maintain the wheel's smooth contour, extending tool life. The negative rake angle of grains results in a bamboo-like chip morphology, which mitigates excessive tool wear by controlling chip deformation. The process also promotes a more uniform stress distribution on γ -TiAl surfaces, reducing the risk of localized tool failure. Overall, UVHEDG enhances tool longevity, reduces abrasive grain loss, and improves grinding stability, making it a superior choice for machining brittle γ -TiAl alloys. In Figure 17a, Liu et al. [156] also studied the tool wear with respect to grinding depth and speed. A comparison between predicted and actual wear rate was presented. It shows that grinding depth increased the wear rate and speed decreases it.

In Figure 17b, a machine learning method to determine the wear ratio is presented [165]. For this purpose, a physical model is compared with the machine learning method in UVAG. The result shows a good agreement between the two methods with a mean error of 0.53–5.2%. This method can provide a knowledge-based rapid method to measure grit wear. In addition to this, Zhang et al. [159] investigated the surface damage mechanism during nanometric cutting of γ -TiAl. The molecular dynamics simulation method was investigated to determine the influence of cutting parameters and pore defect radii on cutting forces, dislocations and stress, etc. The results showed that larger pore defects lead to a more pronounced difference in the studied performance factors. In addition, a “shear-off” phenomenon occurs with a 15Å pore defect and the increasing cutting depth raises the proportion of atoms without pore defects. The study is limited by its use of single-crystal models and the need for further exploration of multi-scale defects in real world conditions.

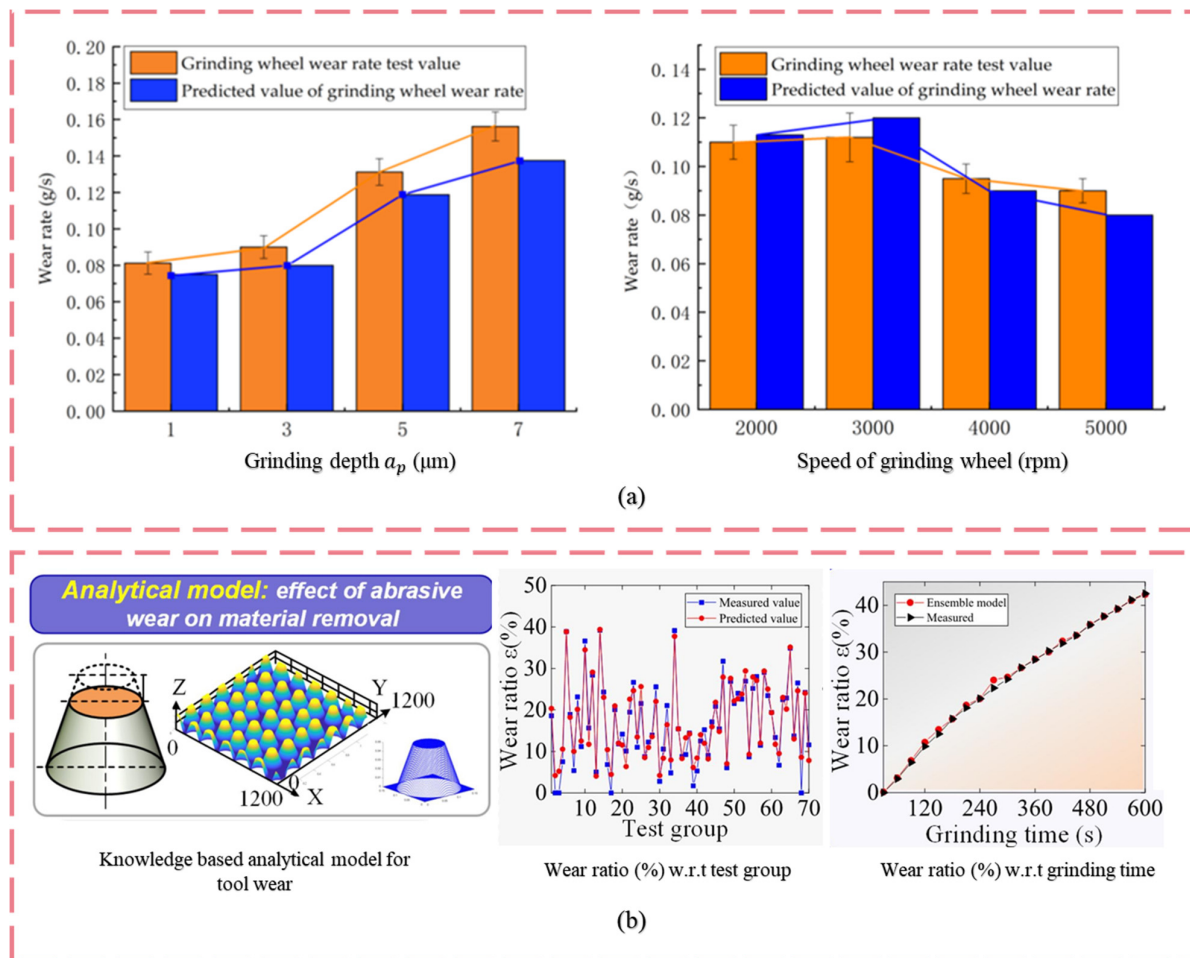


Figure 17. Grinding tool wear VB (a) theoretical vs. experimental wear rate [156] (b) grinding condition under different wear ratio [165].

3.3.4. Influence of UVAG on Surface Integrity

In UVAG application, the material removal characteristics are more distinct compared to conventional grinding [166]. Due to the periodic separation between the tool and the workpiece, the grinding path is interrupted, resulting in shorter and more discontinuous scratches compared to CG, where scratches are longer and continuous [150]. In Figure 18, a similar pattern was observed by Cao et al. [153]. The ultrasonic vibrations enhance the shearing effect and reduce the dominance of plowing, leading to a less severe material deformation and a uniform surface profile. In UVAG, the interrupted cutting action modifies the grinding track with a more irregular and textured surface, while in CG, the grinding track is smoother but affected by material smearing and adhesion [37]. Overall, UVAG enhances material removal efficiency, reduces grinding forces and heat generation, and improves surface integrity, making it advantageous for brittle and hard-to-machine materials like γ -TiAl alloys.

Under conventional grinding, horizontal scratches due to feed rate were observed by Yan et al. [167]. However, the UVAG process shows a sinusoidal horizontal pattern due to its material separation effect that has been discussed earlier. The γ -TiAl has superior strength, but its brittleness creates significant machining challenges. Xia et al. [168] studied the potential of elliptical ultrasonic vibration milling to overcome these challenges and improve machining outcomes. A separation time model was developed to analyze the vibration process in the cutting mechanism. It was determined that periodic brittle fractures

with local dimples indicate material plasticity, causing an 18.17% reduction in cutting force with respect to conventional machining.

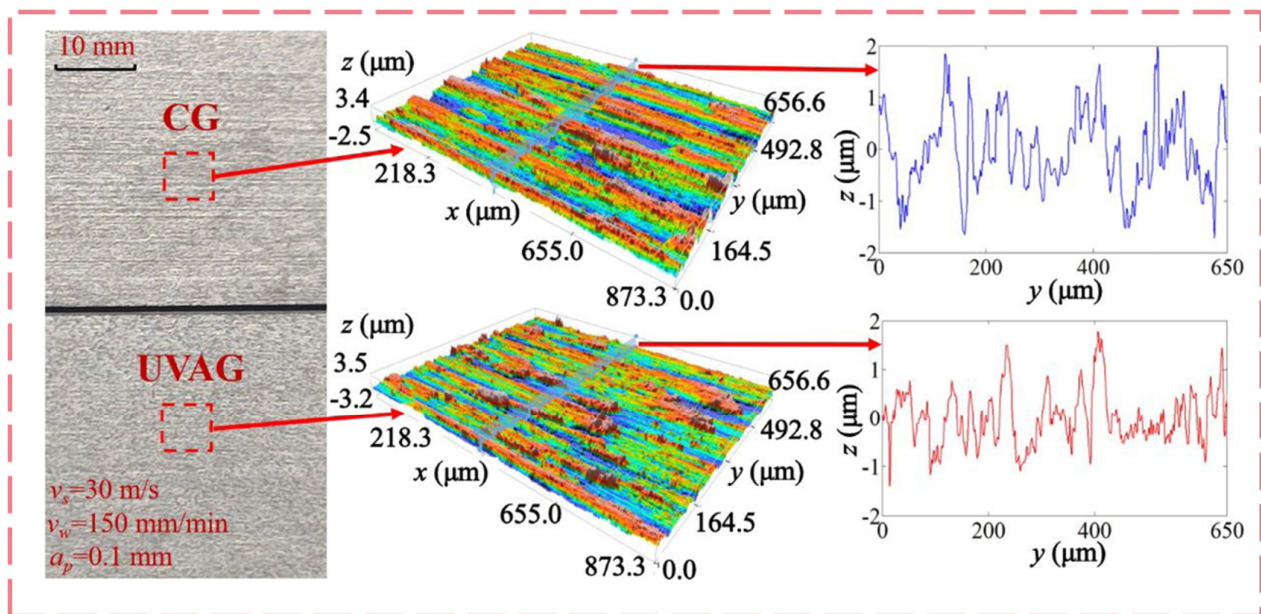


Figure 18. Grinding surface morphology and roughness R_a under UVAG surface profiles [153].

3.4. Comparative Analysis of UAM Methods for Titanium Alloys

The ultrasonic-assisted machining (UAM) methods, i.e., UVAT, UVAG and UVAM offer significant advantages when working with challenging materials like additively manufactured γ -TiAl alloys [169–171]. Traditional methods are less efficient and more prone to tool wear. Therefore, comparative advantages of the UAM methods with conventional machining are presented in Table 6. For example, UVAT utilizes high ultrasonic vibrations to reduce cutting forces during machining [71]. This results in improved surface roughness (R_a), which is significantly better than conventional turning processes [84]. The reduced cutting forces not only minimize tool wear but also enhance dimensional accuracy. As a result, UVAT is suitable for precision turning operations. However, its MRR remains moderate and it is most effective for final operations where fine finishing is required [72,172].

Table 6. Comparative benefits and limitations of UAM in comparison to conventional processes.

Parameter	UVAT	UVAG	UVAM
Surface roughness (R_a , μm)	Improved over conventional	Excellent finish	Moderate to good
Material removal rate (MRR)	Moderate	Low to Moderate	Moderate
Tool wear	Significantly reduced	Reduced (abrasive tool wear controlled)	Reduced (especially in intermittent cuts)
Dimensional accuracy	High	Very high	Moderate to high
Thermal effects	Minimal (due to lower cutting forces)	Very low	Low
Energy consumption	Moderate	Low to moderate	Moderate
Geometric complexity handling	Low to Moderate	Limited	High (due to milling path flexibility)
Suitability for γ -TiAl	Very effective for finishing and precision	Excellent for final surface conditioning	Effective for shallow features and slots

In contrast, UVAG stands out due to its ability to achieve an excellent surface finishing. This method is particularly beneficial for the final surface finish of hard materials like γ -TiAl, where traditional methods often lead to high temperatures, potentially causing cracks or defects on the surface [136]. The UVAG intermittent cutting action reduces grinding forces, leading to lower thermal effects and higher precision. The reduction in grinding forces leads to reduced tool wear and it is especially beneficial for abrasive tools, which tends to degrade quickly under conventional grinding. A significant challenge is the relatively low MRR, which limits its application to finer finishing rather than large-scale material removal [173,174].

UVAM combines the benefits of both turning and grinding but offers flexibility in handling complex geometries and shallow features [120]. It allows for reduced milling forces, minimizing the risk of tool deflection and improving the stability of process. This aspect is valuable in the milling of γ -TiAl, where maintaining cutting precision while managing heat and wear is crucial. The surface roughness achieved with UVAM is generally moderate to good (R_a usually higher than UVAG). Due to this reason, this method is preferred for creating features like slots, pockets and other geometric shapes where conventional milling would struggle due to tool wear and heat buildup.

Overall, UAM methods provide a balanced combination of reduced thermal effects, controlled vibration and increased tool life. Each method has its strengths: UVAT excels in precision finishing, UVAG provides superior surface quality and minimal thermal effect, and UVAM offers versatility for complex geometries. However, the limitations in MRR for these methods highlight the need for further innovation, particularly in hybrid machining processes. The future of γ -TiAl lies in the development of these processes that combine UAM with other processes [129,175–177]. Such a hybridized process could lead to substantial improvements in both production and efficiency, making them ideal for applications where precision and durability are of paramount importance.

4. Emerging Frontiers of UAM

With the advancement of manufacturing technologies and increasing demand for precision machining, UAM has evolved beyond single-mode applications to incorporate multi-energy field strategies. These novel approaches enhance the machinability of hard-to-cut brittle materials by reducing cutting forces, minimizing tool wear and improving surface integrity. Therefore, recent research studies are focusing on predictive models of UAM behavior, ultrasonic/plasma oxidation-assisted machining (UPOAM), hybrid ultrasonic machining with protective coating (HUMPC) and hybrid laser-assisted ultrasonic machining (HLAUM). The emerging frontiers in the field of UAM are outlined in Figure 19.

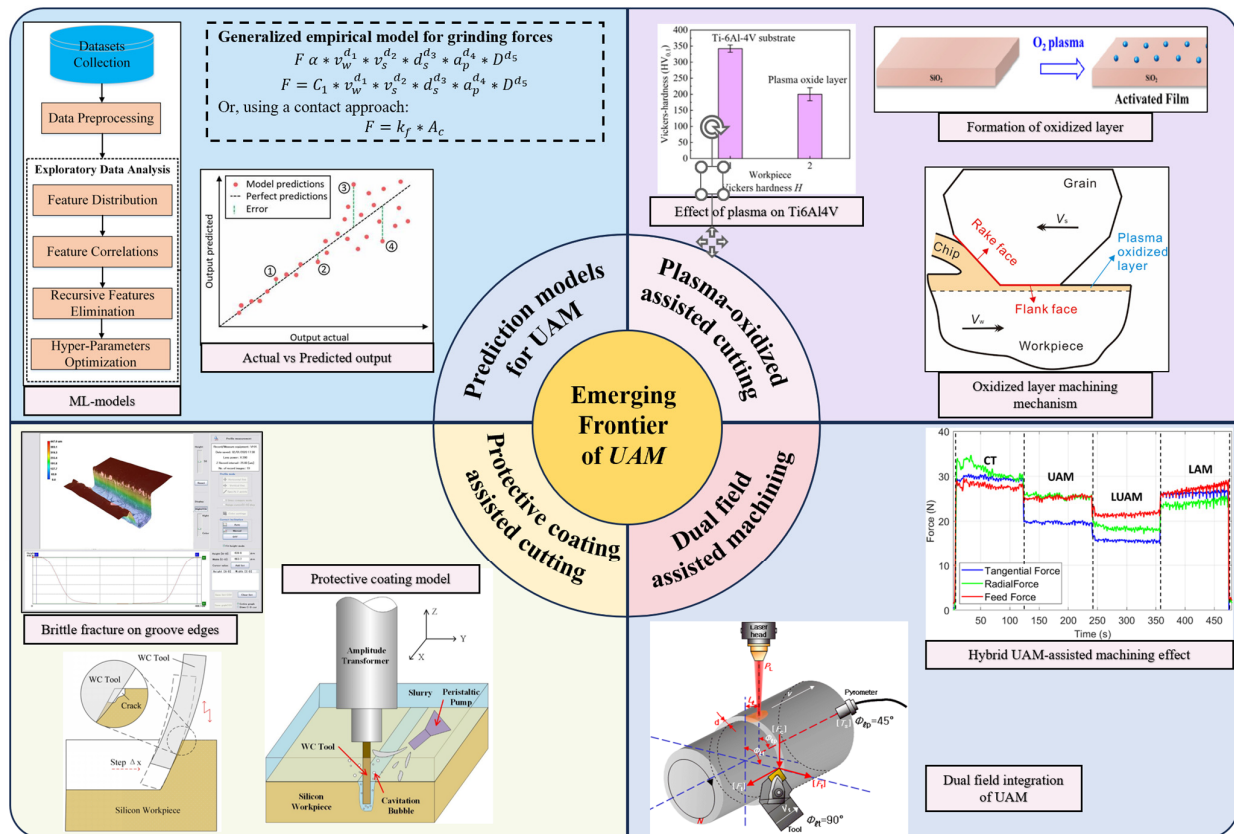


Figure 19. Emerging frontiers of UAM.

4.1. Prediction Model for UAM

The integration of predictive models (cutting force, temperature or machining length) is a key frontier in UAM. These models combine analytical, empirical and computational approaches (e.g., finite element simulations and artificial intelligence) to optimize cutting conditions and tool performance. These models help in understanding the complex interactions between ultrasonic vibrations, material properties and tool dynamics [178,179]. According to Wang et al. [180], a finite element model can be validated through a mechanistic milling force model. This method requires the determination of the cutting force coefficient, which can be obtained by least squares regression. Aydin et al. [181] suggested a mechanical model that also uses related coefficients. However, these coefficients were determined through experimental data. The data were based on cutting force distribution depending on machining conditions.

UAM methods are relatively complex and difficult to control due to high-frequency vibrations and intermittent contact, when compared with conventional methods. The relative motion of tool and workpiece is different in each of these methods. Thus, there is a need for different predictive models for explaining the chip formation behavior [182]. In Table 7, a summary of the predictive models available in the literature is presented. Most of these models are focused on determining the predictive cutting forces. The importance of such models lies in selecting optimal parameters, i.e., cutting speed, feed rate, vibration amplitude and frequency. Predictive cutting forces avoids excessive tool stress and premature failure. It also ensures minimizing cutting forces for better surface quality and reduced subsurface damage. Overall, it enables lower force requirements, reducing energy consumption and improving sustainability in manufacturing.

Table 7. Predictive force models for milling, grinding and turning.

Process	Prediction Model	Ref.
Milling (2D-force model)	$\begin{bmatrix} F_x \\ F_y \end{bmatrix} = \sum_{j=1}^N g(\phi_j(t)) \begin{bmatrix} -\cos\phi_j(t) & -\sin\phi_j(t) \\ \sin\phi_j(t) & -\cos\phi_j(t) \end{bmatrix}$ <p>Whereas, $g(\phi_{-j}(t))$ is the window function.</p>	[183]
Milling (2D-force model)	$F_x = F_u \left[C_1 \frac{f_z}{r} \sin^3\theta + C_2 \frac{f_z}{r} \cos^3\theta - \sin^2\theta + \frac{1}{2} p \sin 2\theta - \frac{f_z}{r} \sin\theta - p\theta \right]_{\theta_s}^{\theta_e}$ $F_y = F_u \left[C_2 \frac{f_z}{r} \sin^3\theta - C_1 \frac{f_z}{r} \cos^3\theta - p \sin^2\theta - \frac{1}{2} \sin 2\theta - p \frac{f_z}{r} \sin\theta - \theta \right]_{\theta_s}^{\theta_e}$ $F_x = -\cos\theta \int [\beta_n D_1 \cos(\beta_n - \alpha) + \tan i_t \tan \eta_c \sin \beta_n + K_{te}] dz$ $- \sin\theta \int \left[\frac{\beta_n D_1}{\cos i_t} \sin(\beta_n - \alpha) + K_{re} \right] dz$	[184]
Milling (3D-force model)	$F_y = \sin\theta \int [\beta_n D_1 \cos(\beta_n - \alpha) + \tan i_t \tan \eta_c \sin \beta_n + K_{te}] dz$ $- \cos\theta \int \left[\frac{\beta_n D_1}{\cos i_t} \sin(\beta_n - \alpha) + K_{re} \right] dz$ $F_z = \int [\beta_n D_1 \cos(\beta_n - \alpha) + \tan i_t \tan \eta_c \sin \beta_n + K_{ae}] dz$ $D_1 = \frac{h_\tau}{\sin\phi \sqrt{\cos^2(\phi + \beta_n - \alpha) + \tan^2 \eta_c \sin^2 \beta_n}}$	[185]
Milling (3D-force model)	$\begin{bmatrix} F_x(\theta) \\ F_y(\theta) \\ F_z(\theta) \end{bmatrix} = \begin{bmatrix} -\cos\theta & -\sin\theta & 0 \\ \sin\theta & -\cos\theta & 0 \\ 0 & 0 & 1 \end{bmatrix}$	[186]
Grinding (cutting)	$F_n = A \left(\frac{C^2}{K_1} \right)^{\frac{1-m}{3}}$	[187]
Grinding (Cutting, plowing, Rubbing)	$F_n = \frac{k_1 \mu_{ch} a_p v_w}{v_s} + k_2 F_{t,p} + p_c \sqrt{d_e a_p} Q$	[188]
Grinding (Cutting, plowing, Rubbing)	$F_n = K \left(\frac{v_w}{v_s} \right) a_p + K_1 \left(\frac{v_w}{v_s} \right) d^{-0.5} a_p^{0.5} + K_4 \left(\frac{v_w}{v_s} \right)^2 d_e^b C_s d_e^{0.5} a_p^{0.5+c}$	[189–191]

Current force and thermal models for UVAM/UVAG remain limited under dynamic and industrial conditions. Most assume steady state cutting, constant vibration parameters, fixed tool geometry and simplified heat partition. Therefore, the effects of transient contact, multi-degree of freedom vibration and contact variability remain unpredicted. This assumption leads to biased force and temperature predictions at production feeds/speed. Future work should integrate coupled structural dynamics and temperature-dependent material laws, and employ probabilistic learning frameworks that can be validated by high standardized benchmarks.

4.2. Hybrid Ultrasonic Machining with Protective Coating (HUMPC)

Brittle materials such as ceramics, glass and silicon wafers pose challenges due to their tendency to fracture under mechanical stress. Hybrid ultrasonic machining with protective coating (HUMPC) involves the application of thin coatings (e.g., TiAlN) that improves thermal stability, impact resistance and lubrication. Their role is to act as a barrier between the tool and the workpiece [192]. Some coatings provide self-lubricating properties, lowering friction and cutting temperatures. These coatings work synergistically with ultrasonic vibrations to minimize crack formation, improve tool life and enhance surface integrity while maintaining the structural integrity of brittle materials [193]. Moreover, the coating reduces tool–workpiece interaction by decreasing the stress concentration at the cutting edges, as depicted in Figure 20. According to Zhao et al. [194], micro-channeling during high-frequency lateral tool motion results in edge breakage and overcutting. This phenomenon was observed for a silicon workpiece with a tungsten–carbide cutting tool. Therefore, a protective layer coating was applied to the surface. It was determined that the machining parameters and the viscosity of it have an impact on the overall performance. A similar characteristic of protective layer was observed by Lan et al. [195] and Yoon et al. [196].

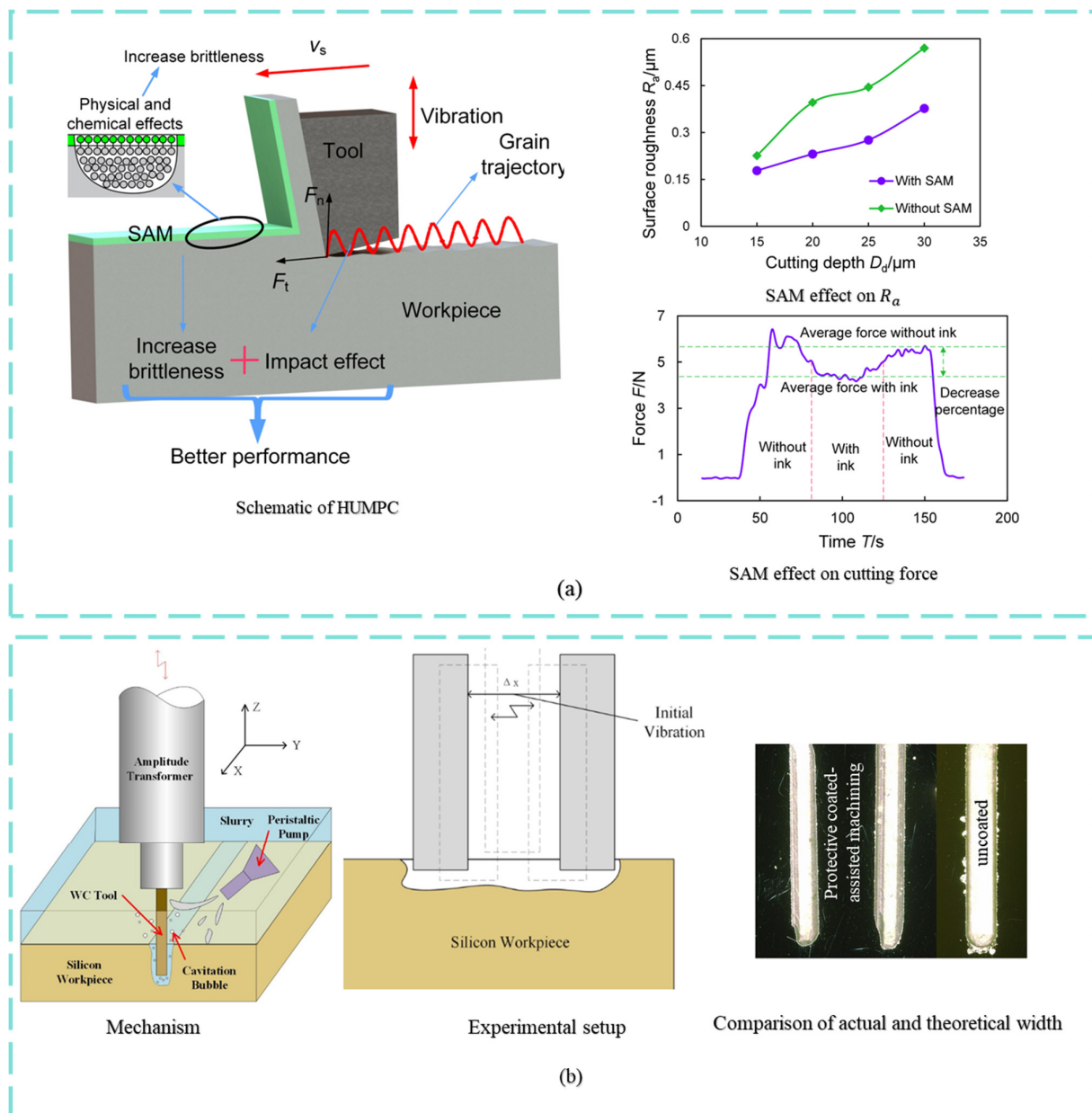


Figure 20. HUMPC machining based on (a) surface active medium (SAM) layer [195] and (b) protective coating for slot edges [194].

4.3. Ultrasonic/Plasma Oxidation-Assisted Machining (UPOAM)

Plasma oxidation has been introduced in UAM to modify the surface properties of materials, reducing their hardness and improving their machinability. This technique creates an oxide layer on the material surface, which acts as a protective barrier, reducing tool wear and cutting forces. When combined with ultrasonic vibration, plasma oxidation enhances chip control, reduces cutting temperatures and improves quality. Therefore, it is highly effective for machining superalloys and titanium-based alloys. According to Wu et al. [197], UPOAM can have significant advantages in improving machining efficiency of Ti6Al4V, as presented in Figure 21. The effect of plasma on Ti6Al4V substrate shows how it can cause a decrease in surface properties. By integrating ultrasonic vibration with plasma oxidation, it can reduce the cutting forces, primarily due to the cavitation effect, which is enhanced by plasma intensity. The authors of [198] also show the potential of UPOAG as a high-efficiency, precision machining technique for titanium alloys.

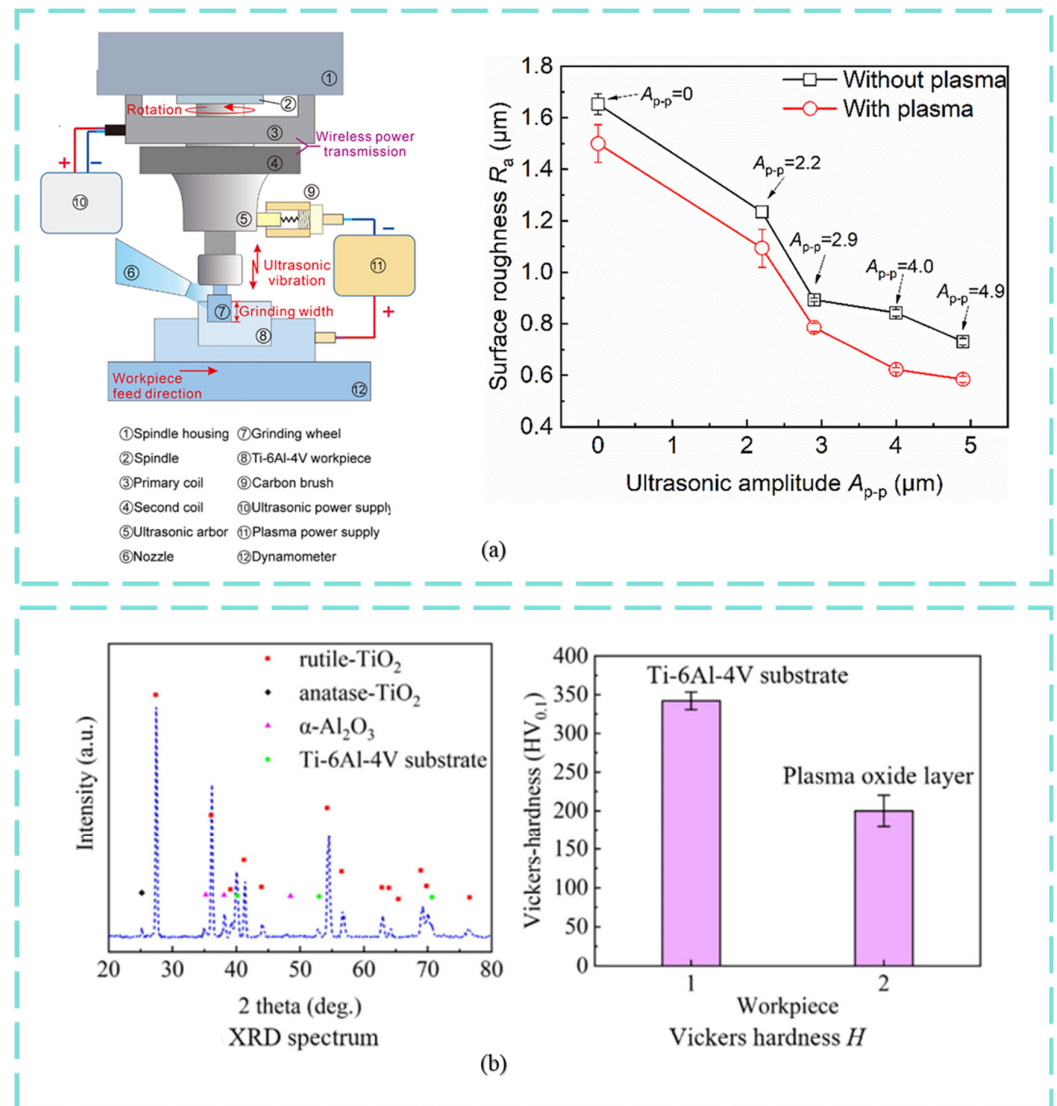


Figure 21. Research status of UPOAM based on (a) benefits of reducing surface roughness [197] and (b) plasma effect on grinding forces [198].

4.4. Dual-Field Integrated Ultrasonic Assisted Machining (DFI-UAM)

As manufacturing demands evolve, dual-field integrated ultrasonic assisted machining (DFI-UAM) presents a transformative approach to overcome machining challenges. By integrating multiple energy fields, such as laser, electrical discharge and magnetic field-assisted techniques, DFI-UAM ensures improved machining accuracy, particularly for aerospace alloys and other hard-to-cut materials. These frontiers pave the way for next generation precision manufacturing, making UAM a cornerstone of advanced machining strategies.

In laser ultrasonic-assisted machining (LUAM), localized laser heating is combined with high-frequency vibrations to enhance the machinability of Ti6Al4V, a challenging alloy [199]. In Figure 22a, a schematic of the process and the combined effect of laser and UAM have been presented by Dominguez-Caballero et al. [200]. In their study, the synergistic effect of using multi-field energies (UAM and laser) was considered beneficial for improving MRR and minimizing tool wear, making it beneficial for titanium alloys. Similarly, Figure 22b shows the mechanism of pulsed-ultrasonic electrical discharge machining (EDM) to enhance machining and precision of finishing operations. According to Goigogana et al. [201], the integration of ultrasonic vibrations with pulsed EDM improves MRR and

enhances surface integrity. The high-frequency vibrations facilitate debris removal and promote uniform energy distribution.

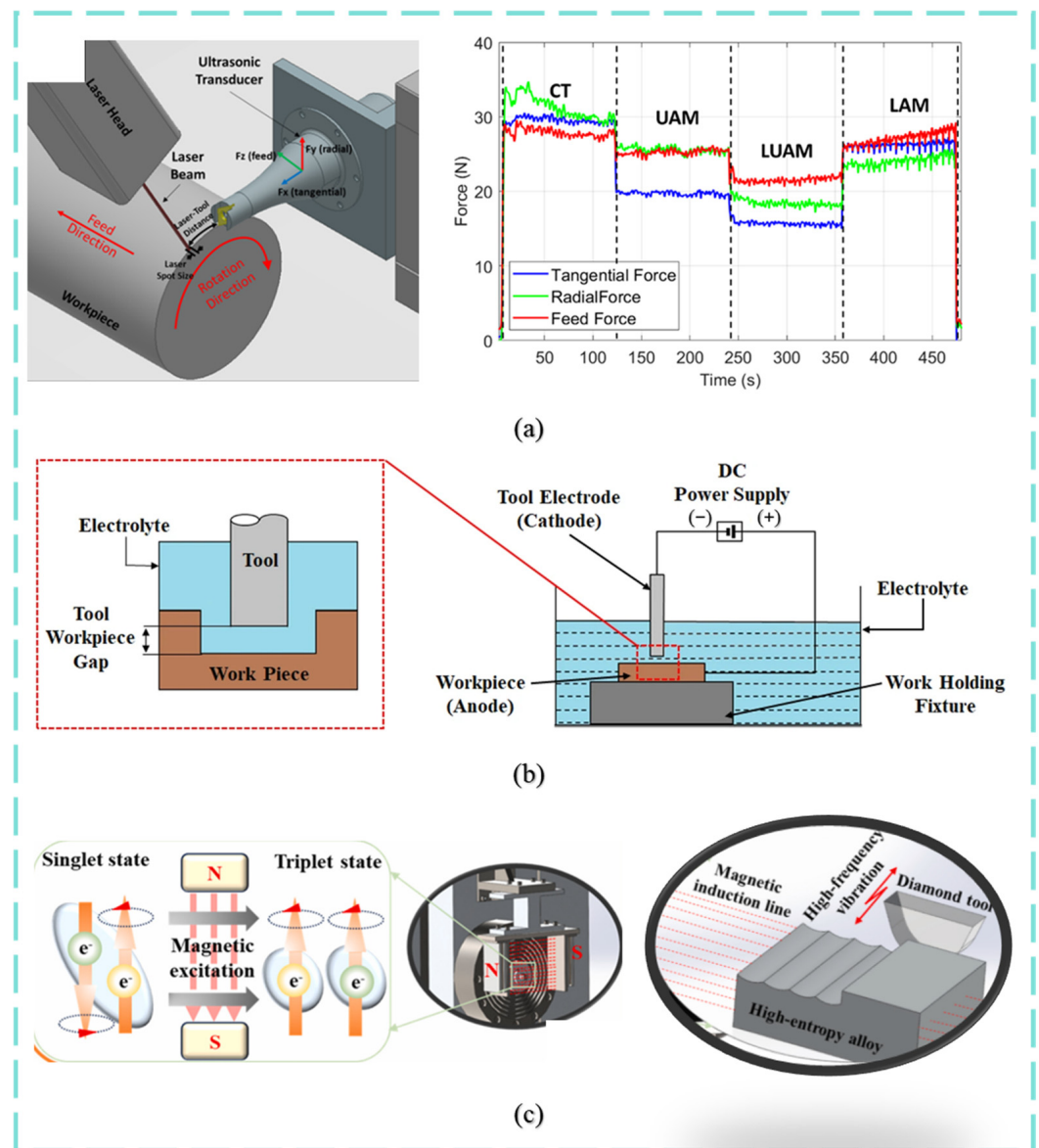


Figure 22. Hybrid machining systems (a) Laser-assisted ultrasonic machining [200], (b) Electrical discharge [202] and (c) Magnetic field-assisted machining [203].

Lastly, the magnetic and ultrasonic-assisted machining (M-UAM) technique is an advanced hybrid approach tailored for high-entropy alloys [204]. According to Xing et al. [203], the M-UAM method enhances material plasticity, reduces cutting forces and improves surface integrity. The magnetic field stabilizes the cutting forces by influencing dislocation movement and thermal effects, while the ultrasonic vibrations promote intermittent cutting, minimizing subsurface damage [205]. Overall, the methods mentioned represent a breakthrough in ultra-precision manufacturing, ensuring enhanced machining.

5. Challenges and Future Outlook

Despite the significant advantages of UAM in enhancing machining efficiency, several challenges hinder its widespread industrial adoption. One major challenge is the complexity of integrating ultrasonic vibration into conventional machining setups while maintaining precise control over amplitude and frequency [51]. Variations in workpiece

material properties, tool geometry and machining parameters can lead to inconsistent results, limiting process reliability. Additionally, high-frequency vibrations induce stress and fatigue issues in the tool, leading to premature wear or even breakage, particularly when machining brittle or high-hardness materials.

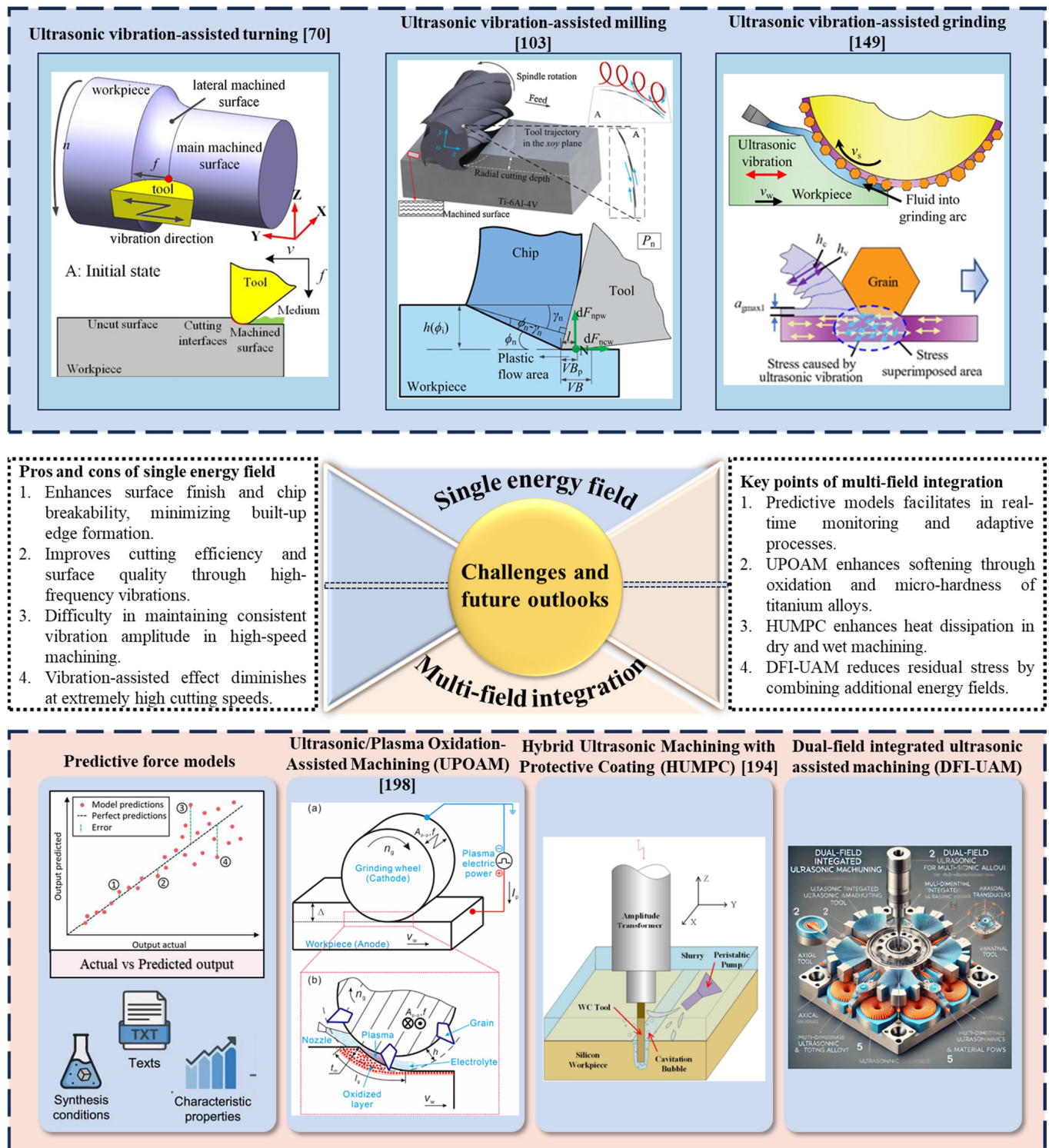


Figure 23. Current and future research prospects.

From an industrial perspective, scalability and cost-effectiveness remain pressing concerns. The integration of ultrasonic modules into high-volume manufacturing lines requires robust and compact systems that can operate reliably under demanding production

conditions. The additional cost of transducers, tool holders and control units must be justified by productivity gains. So far, a comprehensive cost–benefit analysis is still scarce. Furthermore, continuous operations barriers, i.e., fixture stability, heat management and long-term durability pose a significant challenge to industrial deployment. Addressing these challenges will require modular retrofitting solutions, energy-efficient ultrasonic generators and real-time monitoring strategies.

The increasing demand for machining complex and high-performance materials will continue to drive innovations in UAM techniques. Looking ahead, the future of UAM lies in multi-field hybrid machining, where ultrasonic vibration is integrated with other energy fields, i.e., laser, electrical discharge, plasma oxidation and magnetic. In Figure 23, a summary of current and future research prospects of UAM technology has been outlined. It is evident that the development of predictive models and Artificial Intelligence (AI)-based optimization algorithms will enhance process control. Consequently, UAM is made more adaptive and efficient for diverse applications. Additionally, advancements in high-speed imaging and acoustic emission sensors will enable better process optimization and defect detection [10,53,206,207]. Overall, as automation and digital manufacturing technologies evolve, UAM is expected to become a key enabler of next-generation precision manufacturing.

6. Conclusions

In conclusion, ultrasonic-assisted machining (UAM) has proven to be an effective approach for improving the machinability of titanium–aluminum (TiAl) alloys, which are difficult to process. Techniques such as ultrasonic-assisted turning (UVAT), milling (UVM) and grinding (UVAG) have demonstrated significant improvements in material removal, efficiency, surface quality and tool life. However, this review highlighted the limitations of these single-energy field UAM techniques, including the inconsistencies, which have driven the need for the development of multi-field and hybrid strategies. Advanced approaches, including ultrasonic-plasma oxidation-assisted grinding and dual field integrations, present promising avenues for further enhancing TiAl processing. Overall, this review not only evaluates the characterization, machining efficiency and emerging trends in UAM for TiAl, but also outlines the challenges and future outlook. This aims to guide both future research and industrial applications in high-performance material processing.

Author Contributions: M.F.J.: Methodology, Software, Validation, Investigation, Data Curation, Writing—Original Draft and Editing; Q.L.: Methodology, Experiment. M.K.: Methodology, Validation; P.F.: Supervision, Funding acquisition; J.Z.: Supervision, Methodology, Visualization, Writing—Review and Editing. All authors have read and agreed to the published version of the manuscript.

Funding: This research was funded by the National Natural Science Foundation of China (Grant No. 52275441 and 52105458); the Natural Science Foundation of Beijing (Grant No. 3222009).

Data Availability Statement: All relevant data and material are visible in the manuscript.

Conflicts of Interest: The authors declare that they have no known competing financial interests or personal relationships that could have appeared to influence the work reported in this paper. The authors declare no conflicts of interest.

Abbreviations

UVAM	Ultrasonic-assisted machining	CM	Conventional machining
GMA	Gas metal arc	AUVAT	axial ultrasonic vibration assisted turning
UVAT	Ultrasonic vibration assisted turning	RUVAT	Radial ultrasonic vibration assisted turning
BUE	built-up-edge	MQL	Minimum quantity lubrication
LCO ₂	liquid carbon dioxide	SEM	Scanning electron microscope
E-UVAT	Elliptical ultrasonic vibration-assisted turning	UVAM	ultrasonic vibration-assisted milling
MRR	Material removal rate	L-UVAM	Longitudinal ultrasonic vibration-assisted milling
FD-UVAM	feed direction ultrasonic vibration-assisted milling	LT-UVAM	longitudinal torsional ultrasonic vibration-assisted milling
UVHEDG	Ultrasonic vibration-assisted high-efficiency deep grinding	UVAG	Ultrasonic vibration-assisted grinding
DFI-UAM	Dual-field integrated ultrasonic assisted machining	HUMPC	Hybrid Ultrasonic Machining with Protective Coating
UPOAM	Ultrasonic/Plasma Oxidation-Assisted Machining	LUAM	Laser-ultrasonic assisted machining
EDM	Electrical discharge machining	(M-UAM)	magnetic and ultrasonic-assisted machining
TiAl	Titanium aluminide	AI	Artificial intelligence
F_t & F_n	Tangential and normal force (N)	α & β	Angular functions
FEM	finite element method	F_x, F_y, F_z	Force in x, y and z direction (N)
VB	Tool wear (mm)	S_a	Arithmetic means of 3D surface roughness
R_a	Arithmetic mean of 2D surface roughness	T_c	Cutting temperature (°C)
F_R	Resultant force (N)	TL	Tool life
σ_R	Residual stress (MPa)	f	Feed rate
F_u	Mean force (N)	$g(\phi_j(t))$	Window function
C_1 & C_2	Material constants	d_e	Diameter (m)

References

1. Fatemi, A.; Molaei, R.; Sharifimehr, S.; Phan, N.; Shamsaei, N. Multiaxial fatigue behavior of wrought and additive manufactured Ti-6Al-4V including surface finish effect. *Int. J. Fatigue* **2017**, *100*, 347–366. [\[CrossRef\]](#)
2. Xiao, G.; Zhang, Y.; Huang, Y.; Song, S.; Chen, B. Grinding mechanism of titanium alloy: Research status and prospect. *J. Adv. Manuf. Sci. Technol.* **2021**, *1*, 2020001. [\[CrossRef\]](#)
3. Khan, A.; Wang, X.; Zhao, B.; Ding, W.; Jamil, M.; Khan, A.M.; Ali, S.H.; Hussain, S.; Zhang, J.; Das, R. Ultrasonic vibration-assisted cutting of titanium alloys: A state-of-the-art review. *Chin. J. Aeronaut.* **2024**, *38*, 103078. [\[CrossRef\]](#)
4. Mi, G.; Sun, R.; Wu, M.; Tan, Y.; Qiu, Y.; Li, P. Research progress of molecular dynamic calculation on titanium alloys for aero-engine. *J. Aeronaut. Mater.* **2024**, *44*, 87–103. [\[CrossRef\]](#)
5. Festas, A.; Ramos, A.; Davim, J.P. Machining of titanium alloys for medical application—A review. *Proc. Inst. Mech. Eng. Part B J. Eng. Manuf.* **2022**, *236*, 309–318. [\[CrossRef\]](#)
6. Shu, T.; Shi, H.; Li, M.; Lin, Y.-C.; Li, A.; Pei, D. Microscale bone interlocking enhances osseointegration strength on the rough surface of 3D-printed titanium implants: Experimental and finite element analysis. *BMC Oral Health* **2025**, *25*, 208. [\[CrossRef\]](#) [\[PubMed\]](#)
7. Chtioui, A.; Oubalouch, A.; Mouchtachi, A. Evolution of the chip morphology during high speed machining of titanium alloy. *AIP Conf. Proc.* **2024**, *3241*, 020001.
8. Du, H.; Chen, H.; Zhu, Z.; Wang, Z.; To, S. Novel hybrid machining process of titanium alloy for texturing high-quality microstructure array surfaces. *Surf. Coat. Technol.* **2023**, *462*, 129494. [\[CrossRef\]](#)
9. Kostov, A.; Živković, D. Thermodynamic analysis of alloys Ti–Al, Ti–V, Al–V and Ti–Al–V. *J. Alloys Compd.* **2008**, *460*, 164–171. [\[CrossRef\]](#)
10. Duman, E.; Yapan, Y.F.; Uysal, A.; Sofuoğlu, M.A. Ultrasonic vibration-assisted machining with minimum quantity lubrication for aerospace materials. In *Advances in Manufacturing for Aerospace Alloys*; Springer Nature: Cham, Switzerland, 2024; pp. 47–76.

11. Ellard, J.; Mathabathe, M.; Siyasiya, C.; Bolokang, A.; Vilane, V.; Rikhotso-Mbungela, R.; McDuling, C.; Masete, S. Engineering γ -TiAl alloys: The effects of Sn, Si and Mn on densification, microstructure, and mechanical properties. *Intermetallics* **2025**, *181*, 108746. [\[CrossRef\]](#)
12. Lu, Q.; Zheng, M.; Zhu, Z.; Chen, W.; Tan, H.; Song, B. Tribological behavior of duplex titanium-aluminum alloys at the nanoscale under different vibration amplitudes. *Phys. Scr.* **2025**, *100*, 055405. [\[CrossRef\]](#)
13. Yang, Z.; Zhu, L.; Zhang, G.; Ni, C.; Lin, B. Review of ultrasonic vibration-assisted machining in advanced materials. *Int. J. Mach. Tools Manuf.* **2020**, *156*, 103594. [\[CrossRef\]](#)
14. Manikandan, P.; Venkatesan, K. Advancements in micromachining of additive manufactured materials: A comprehensive review. *Mater. Manuf. Process.* **2024**, *39*, 1469–1520. [\[CrossRef\]](#)
15. Hémery, S.; Naït-Ali, A.; Smerdova, O.; Tromas, C. Deformation mechanisms in the α phase of the Ti-6Al-2Sn-4Zr-2Mo titanium alloy: In situ experiments and simulations. *Int. J. Plast.* **2024**, *175*, 103947. [\[CrossRef\]](#)
16. Duan, B.; Yang, Y.; He, S.; Feng, Q.; Mao, L.; Zhang, X.; Jiao, L.; Lu, X.; Chen, G.; Li, C. History and development of γ -TiAl alloys and the effect of alloying elements on their phase transformations. *J. Alloys Compd.* **2022**, *909*, 164811. [\[CrossRef\]](#)
17. Feng, L.; Li, B.; Li, Q.; Gao, Y.; Pei, Z.; Liang, C. Enhancement of mechanical properties and oxidation resistance of TiAl alloy with addition of Nb and Mo alloying elements. *Mater. Chem. Phys.* **2024**, *316*, 129148. [\[CrossRef\]](#)
18. Huang, S.; Lin, Y.-C.; Chung, R.-J. A Review of the State of Art of Fabrication Technologies of Titanium Aluminide (Ti-Al) Based on US Patents. *Metals* **2024**, *14*, 418. [\[CrossRef\]](#)
19. Najafizadeh, M.; Yazdi, S.; Bozorg, M.; Ghasempour-Mouziraji, M.; Hosseinzadeh, M.; Zarrabian, M.; Cavaliere, P. Classification and applications of titanium and its alloys: A review. *J. Alloys Compd. Commun.* **2024**, *3*, 100019. [\[CrossRef\]](#)
20. Xue, H.; Song, Y.; Tong, X.; Liang, Y.; Peng, H.; Wang, Y.; Shang, S.-L.; Liu, Z.-K.; Lin, J. Enhancing strength and ductility in high Nb-containing TiAl alloy additively manufactured via directed energy deposition. *Addit. Manuf.* **2024**, *86*, 104194. [\[CrossRef\]](#)
21. Xu, S.-H.; Lan, J.-J.; Han, M.; Zhang, H.-B.; Shen, K.-J.; Lin, J.-P.; Cao, H.-Z.; Zheng, G.-Q. Effect of rhenium addition on microstructure and mechanical properties of Ti-48Al-2Cr-2Nb alloys. *Trans. Nonferrous Met. Soc. China* **2025**, *35*, 474–485. [\[CrossRef\]](#)
22. Xiong, J.; Liu, G.; Zhang, G. Influence of interlayer temperature on microstructure and mechanical properties of TiAl alloys in wire and arc additive manufacturing. *J. Manuf. Process.* **2023**, *94*, 278–288. [\[CrossRef\]](#)
23. He, T.; Yi, B.; Zheng, M.; Song, B.; Qu, D.; Chen, J.; Zhu, Z. Molecular dynamics for nanoindentation in the γ/α_2 interfacial strengthening mechanism of a duplex full lamellar TiAl alloy. *Mater. Today Commun.* **2024**, *38*, 107965. [\[CrossRef\]](#)
24. Wang, X.; Guo, R.; Liu, G.; Li, T.; Yang, Y.; Chen, Y.; Xin, M.; Wang, Z. Microstructure Characteristics and Elevated Temperature Mechanical Properties of a B Contained β -solidified γ -TiAl Alloy. *J. Wuhan Univ. Technol. Sci. Ed.* **2024**, *39*, 738–746. [\[CrossRef\]](#)
25. Wang, X.; He, Q.-L.; Zhao, B.; Ding, W.-F.; Liu, Q.; Xu, D.-D. Effects of tool coating and tool wear on the surface and chip morphology in side milling of Ti2AlNb intermetallic alloys. *Adv. Manuf.* **2025**, *13*, 155–166. [\[CrossRef\]](#)
26. Wang, X.; Qu, F.; Qiu, C. On the Microstructural Evolution and Cracking Behavior of a Titanium Aluminide Alloy During Selective Laser Melting. *3D Print. Addit. Manuf.* **2024**, *11*, 40–49. [\[CrossRef\]](#) [\[PubMed\]](#)
27. Liu, H.; Yu, H.; Guo, C.; Chen, X.; Zhong, S.; Zhou, L.; Osman, A.; Lu, J. Review on fatigue of additive manufactured metallic alloys: Microstructure, performance, enhancement, and assessment methods. *Adv. Mater.* **2024**, *36*, e2306570. [\[CrossRef\]](#)
28. Polishetty, A.; Shunmugavel, M.; Goldberg, M.; Littlefair, G.; Singh, R.K. Cutting force and surface finish analysis of machining additive manufactured titanium alloy Ti-6Al-4V. *Procedia Manuf.* **2017**, *7*, 284–289. [\[CrossRef\]](#)
29. Wimler, D.; Lindemann, J.; Kremmer, T.; Clemens, H.; Mayer, S. Microstructure and mechanical properties of novel TiAl alloys tailored via phase and precipitate morphology. *Intermetallics* **2021**, *138*, 107316. [\[CrossRef\]](#)
30. Zhang, H.; Yan, N.; Liang, H.; Liu, Y. Phase transformation and microstructure control of Ti2AlNb-based alloys: A review. *J. Mater. Sci. Technol.* **2021**, *80*, 203–216. [\[CrossRef\]](#)
31. Illarionov, A.G.; Stepanov, S.I.; Naschetnikova, I.A.; Popov, A.A.; Soundappan, P.; Thulasi Raman, K.H.; Suwas, S. A review—Additive manufacturing of intermetallic alloys based on orthorhombic titanium aluminide Ti₂AlNb. *Materials* **2023**, *16*, 991. [\[CrossRef\]](#)
32. Cebi, A.; Nesli, S.; Aslan, M.T.; Yilmaz, O.; Demirtas, H.; Subasi, L.; Gunaydin, A.; Bilgin, G.M.; Orhangul, A.; Akbulut, G. Surface characteristics of additively manufactured γ -TiAl intermetallic alloys post-processed by electrochemical machining. *Surfaces Interfaces* **2024**, *49*, 104381. [\[CrossRef\]](#)
33. Kalita, D.; Rogal, Ł.; Czeppe, T.; Wójcik, A.; Kolano-Burian, A.; Zackiewicz, P.; Kania, B.; Dutkiewicz, J. Microstructure and mechanical properties of Ti-Nb alloys prepared by mechanical alloying and spark plasma sintering. *J. Mater. Eng. Perform.* **2020**, *29*, 1445–1452. [\[CrossRef\]](#)
34. Chen, H.; Hu, S.; Wang, L.; Deng, L. Directional design and preparation of Ti-Nb based alloys with predicted high strength and low modulus for biomedical applications: Insights from first-principles calculations. *Intermetallics* **2025**, *177*, 108580. [\[CrossRef\]](#)
35. Yang, Y.; Chen, Y.; Gesang, Y.; Pan, M.; Liang, Y. Tribological properties of γ -TiAl alloy fretting against nickel-based superalloy at elevated temperature. *Tribol. Trans.* **2024**, *67*, 259–269. [\[CrossRef\]](#)

36. Bugvi, S.A.; Mughal, K.H.; Jamil, M.F.; Kazim, A.H.; Shabbir, A.; Shahid, M.U.; Dar, M.U.; Asif, M.M.; Imran, H. Evaluating the work design readiness for industry 4.0 based on personal characteristics of production workers. *Int. J. Ind. Eng.* **2024**, *31*, 2. [\[CrossRef\]](#)
37. Yang, S.; Zhang, G.; Xiao, G. Parameter optimization for ultrasonic-assisted grinding of γ -TiAl intermetallics: A gray relational analysis approach with surface integrity evaluation. *Rev. Adv. Mater. Sci.* **2024**, *63*, 20240045. [\[CrossRef\]](#)
38. Ahmad, N.; Irfan, S.; Maleki, E.; Lee, S.; Liu, J.P.; Shao, S.; Shamsaei, N. Determining critical surface features affecting fatigue behavior of additively manufactured Ti-6Al-4V. *Int. J. Fatigue* **2025**, *197*, 108956. [\[CrossRef\]](#)
39. Assis, J.O.M.; Lauro, C.H.; Pereira, R.B.D.; Brandão, L.C.; Arruda, É.M.; Davim, J.P. A Chip Formation Study of the Micro-Cutting of Commercially Pure Titanium. *Metals* **2024**, *14*, 851. [\[CrossRef\]](#)
40. Attar, H.; Bermingham, M.; Ehtemam-Haghighi, S.; Dehghan-Manshadi, A.; Kent, D.; Dargusch, M. Evaluation of the mechanical and wear properties of titanium produced by three different additive manufacturing methods for biomedical application. *Mater. Sci. Eng. A* **2019**, *760*, 339–345. [\[CrossRef\]](#)
41. Li, G.; Chandra, S.; Rashid, R.A.R.; Palanisamy, S.; Ding, S. Machinability of additively manufactured titanium alloys: A comprehensive review. *J. Manuf. Process.* **2022**, *75*, 72–99. [\[CrossRef\]](#)
42. Zhang, H.; Dang, J.; Ming, W.; Xu, X.; Chen, M.; An, Q. Cutting responses of additive manufactured Ti6Al4V with solid ceramic tool under dry high-speed milling processes. *Ceram. Int.* **2020**, *46*, 14536–14547. [\[CrossRef\]](#)
43. Zhang, P.; Zhou, H.; Ge, S.; Sun, Y.; Zhang, J. Research on nanocutting mechanism of polycrystalline γ -TiAl alloy at different temperatures. *Vacuum* **2024**, *230*, 113734. [\[CrossRef\]](#)
44. Zhang, S.; Jiang, H.; Xin, J.; Zhang, Y.; Zhu, Z.; Tian, S. The investigation of high-temperature shear deformation mechanism in Ti-44Al-4Nb-1.5Mo-0.1B alloy. *Mater. Sci. Eng. A* **2025**, *934*, 148298. [\[CrossRef\]](#)
45. Zhou, Y.; Cao, H.; Zhou, B.; Li, H.; Chen, W.; Lei, C.; Feng, R. Molecular dynamics simulation of the effect of tool parameters on nano-cutting of polycrystalline γ -TiAl alloys. *Model. Simul. Mater. Sci. Eng.* **2024**, *32*, 065005. [\[CrossRef\]](#)
46. Aspinwall, D.; Dewes, R.; Mantle, A. The machining of γ -TiAl intermetallic alloys. *CIRP Ann.* **2005**, *54*, 99–104. [\[CrossRef\]](#)
47. Liu, X.; Liu, H.; Shi, S.; Tang, Y.; Zhang, J. On revealing the mechanisms involved in brittle-to-ductile transition of fracture behaviors for γ -TiAl alloy under dynamic conditions. *J. Alloys Compd.* **2025**, *1010*, 177614. [\[CrossRef\]](#)
48. Zhang, S.; Tian, N.; Li, D.; Li, J.; Jin, F.; Wang, G.; Tian, S. Microstructure evolution and fracture mechanism of a TiAl–Nb alloy during high-temperature tensile testing. *Mater. Sci. Eng. A* **2022**, *831*, 142094. [\[CrossRef\]](#)
49. Zhang, P.; Zhou, H.; Sun, Y.; Zhang, J.; Yue, X.; Wang, Y. Investigation on the surface damage mechanism of single-crystal γ -TiAl alloy with pore defects based on nanocutting. *Vacuum* **2024**, *229*, 113613. [\[CrossRef\]](#)
50. Sahto, M.P.; Wei, W.; Jamil, M.F.; Mehmood, A.; Sattar, M.; Raza, A.; Rahman, M.U.; Qaisrani, M.A. Integrating experimental and theoretical investigations of porous graphite materials with scanning electron microscope image processing. *Results Eng.* **2024**, *24*, 102893. [\[CrossRef\]](#)
51. Brehl, D.E.; Dow, T.A. Review of vibration-assisted machining. *Precis. Eng.* **2008**, *32*, 153–172. [\[CrossRef\]](#)
52. Chen, Y.; Zhou, B.; Zhu, H.; Li, H.; Feng, R.; Cao, H.; Lei, C. Effect of UEVC parameters on cutting surface quality and subsurface damage of single crystal γ -TiAl alloy via atomic simulation. *Model. Simul. Mater. Sci. Eng.* **2024**, *32*, 065032. [\[CrossRef\]](#)
53. Gupta, M.K.; Korkmaz, M.E.; Yilmaz, H.; Şirin, Ş.; Ross, N.S.; Jamil, M.; Królczyk, G.M.; Sharma, V.S. Real-time monitoring and measurement of energy characteristics in sustainable machining of titanium alloys. *Measurement* **2024**, *224*, 113937. [\[CrossRef\]](#)
54. Gupta, M.K.; Song, Q.; Liu, Z.; Pruncu, C.I.; Mia, M.; Singh, G.; Lozano, J.A.; Carou, D.; Khan, A.M.; Jamil, M.; et al. Machining characteristics based life cycle assessment in eco-benign turning of pure titanium alloy. *J. Clean. Prod.* **2020**, *251*, 119598. [\[CrossRef\]](#)
55. Yip, W.S.; To, S.; Zhou, H.; Ren, J. *Sustainable Machining and Micro-Machining*; Springer Nature: Dordrecht, The Netherlands, 2025. [\[CrossRef\]](#)
56. Wang, X.; Song, J.; Xiao, H.; Liang, Z.; Qin, X.; Chen, T.; Ding, W.; Zhao, B. Wear behavior and material removal mechanism during ultrasonic vibration-assisted grinding γ -TiAl materials using a single CBN grain. *Int. J. Adv. Manuf. Technol.* **2025**, *137*, 1581–1598. [\[CrossRef\]](#)
57. Mughal, K.H.; Ahmad, N.; Hayat, N.; Qureshi, M.A.M.; Bugvi, S.A.; Jamil, M.F.; Khan, M.A. Design and performance evaluation of a novel ultrasonic welding sonotrode for Langevin transducer using finite element approach. *Int. J. Ind. Eng.* **2023**, *30*, 4. [\[CrossRef\]](#)
58. Mughal, K.H.; Bugvi, S.A.; Jamil, M.F.; Qureshi, M.A.M.; Khalid, F.A.; Qaiser, A.A. Tubular cubic polynomial sonotrode for green and sustainable ultrasonic welding technology. *Green Manuf. Open* **2023**, *1*, 14. [\[CrossRef\]](#)
59. Mughal, K.H.; Jamil, M.F.; Qureshi, M.A.M.; Qaiser, A.A.; Khalid, F.A.; Maqbool, A.; Raza, S.F.; Ahmad, S.; Zhang, J.; Abbas, S.Z. Investigation of rotary ultrasonic vibration assisted machining of Nomex honeycomb composite structures. *Int. J. Adv. Manuf. Technol.* **2023**, *129*, 5541–5560. [\[CrossRef\]](#)
60. Mughal, K.H.; Qureshi, M.A.M.; Jamil, M.F.; Ahmad, S.; Khalid, F.A.; Qaiser, A.A.; Maqbool, A.; Raza, S.F.; Zhang, J. Investigation of hybrid ultrasonic machining process of Nomex honeycomb composite using a toothed disc cutter. *Ultrasonics* **2024**, *141*, 107343. [\[CrossRef\]](#)

61. Liu, Y.; Liu, L.; Li, H.; Zhou, B.; Cao, H.; Feng, R. Effect of repetitive nano-cutting tool parameters on surface quality and subsurface damage of γ -TiAl alloy. *Model. Simul. Mater. Sci. Eng.* **2024**, *32*, 045005. [\[CrossRef\]](#)
62. Jiang, Q.; Hua, Y.; Liu, X.; Li, L.; Zhang, J.; Li, F.; Han, J.; Li, Z. Cutting mechanism of laser-ultrasonic-vibration assisted machining of Ti6Al4V under two chip states based on FEM model. *Int. J. Adv. Manuf. Technol.* **2025**, *137*, 2267–2291. [\[CrossRef\]](#)
63. Namlu, R.H.; Lotfi, B.; Kiliç, S.E. Enhancing machining efficiency of Ti-6Al-4V through multi-axial ultrasonic vibration-assisted machining and hybrid nanofluid minimum quantity lubrication. *J. Manuf. Process.* **2024**, *119*, 348–371. [\[CrossRef\]](#)
64. Nasr, M.M.; Anwar, S. Developing an intelligent approach based on ANFIS and advanced NSGA-III for improving the turning performance of additively manufactured γ -TiAl alloy. *Int. J. Adv. Manuf. Technol.* **2025**, *137*, 3333–3358. [\[CrossRef\]](#)
65. Wei, S.; Zou, P.; Fang, L.; Duan, J. Theoretical and experimental study of 3D ultrasonic vibration-assisted turning driven by two actuators. *Measurement* **2023**, *215*, 112865. [\[CrossRef\]](#)
66. Sui, H.; Zhang, L.; Wang, S.; Gu, Z. Transient separation cutting characteristic of axial ultrasonic vibration-assisted cutting. *Int. J. Adv. Manuf. Technol.* **2020**, *110*, 2407–2425. [\[CrossRef\]](#)
67. Kurniawan, R.; Ahmed, F.; Ali, S.; Park, G.C.; Ko, T.J. Analytical, FEA, and experimental research of 2D-Vibration Assisted Cutting (2D-VAC) in titanium alloy Ti6Al4V. *Int. J. Adv. Manuf. Technol.* **2021**, *117*, 1739–1764. [\[CrossRef\]](#)
68. Airao, J.; Nirala, C.K.; Bertolini, R.; Krolczyk, G.M.; Khanna, N. Sustainable cooling strategies to reduce tool wear, power consumption and surface roughness during ultrasonic assisted turning of Ti-6Al-4V. *Tribol. Int.* **2022**, *169*, 107494. [\[CrossRef\]](#)
69. Tan, R.; Zhao, X.; Guo, S.; Zou, X.; He, Y.; Geng, Y.; Hu, Z.; Sun, T. Sustainable production of dry-ultra-precision machining of Ti-6Al-4V alloy using PCD tool under ultrasonic elliptical vibration-assisted cutting. *J. Clean. Prod.* **2020**, *248*, 119254. [\[CrossRef\]](#)
70. Zhang, X.; Peng, Z.; Li, Z.; Sui, H.; Zhang, D. Influences of machining parameters on tool performance when high-speed ultrasonic vibration cutting titanium alloys. *J. Manuf. Process.* **2020**, *60*, 188–199. [\[CrossRef\]](#)
71. Airao, J.; Nirala, C.K. Machinability of Ti-6Al-4V and Nimonic-90 in ultrasonic-assisted turning under sustainable cutting fluid. *Mater. Today Proc.* **2022**, *62*, 7396–7400. [\[CrossRef\]](#)
72. Yan, L.; Zhang, Q.; Yu, J. Effects of continuous minimum quantity lubrication with ultrasonic vibration in turning of titanium alloy. *Int. J. Adv. Manuf. Technol.* **2018**, *98*, 827–837. [\[CrossRef\]](#)
73. Silberschmidt, V.V.; Mahdy, S.M.; Gouda, M.A.; Naseer, A.; Maurotto, A.; Roy, A. Surface-roughness improvement in ultrasonically assisted turning. *Procedia CIRP* **2014**, *13*, 49–54. [\[CrossRef\]](#)
74. Peng, Z.; Zhang, X.; Liu, L.; Xu, G.; Wang, G.; Zhao, M. Effect of high-speed ultrasonic vibration cutting on the microstructure, surface integrity, and wear behavior of titanium alloy. *J. Mater. Res. Technol.* **2023**, *24*, 3870–3888. [\[CrossRef\]](#)
75. Chen, F.; Wang, D.; Wu, S. Influence of ultrasonic vibration-assisted cutting on ploughing effect in cutting Ti6Al4V. *Arch. Civ. Mech. Eng.* **2021**, *21*, 42. [\[CrossRef\]](#)
76. Chen, D.; Chen, J.; Zhou, H. The finite element analysis of machining characteristics of titanium alloy in ultrasonic vibration assisted machining. *J. Mech. Sci. Technol.* **2021**, *35*, 3601–3618. [\[CrossRef\]](#)
77. Lotfi, M.; Amini, S.; Akbari, J. Surface integrity and microstructure changes in 3D elliptical ultrasonic assisted turning of Ti-6Al-4V: FEM and experimental examination. *Tribol. Int.* **2020**, *151*, 106492. [\[CrossRef\]](#)
78. Ingle, S.; Raut, D. Evaluation of tool wears mechanism considering machining parameters and performance parameters for titanium alloy in turning operation on CNC. *Adv. Mater. Process. Technol.* **2024**, *10*, 1380–1400. [\[CrossRef\]](#)
79. Qiu, W.; Pan, D.; Li, J.; Guo, P.; Qiao, Y.; Wang, X. Chip formation mechanism in cryogenic machining of high temperature alloy-Inconel 718 and Ti-47.5Al-2.5V-1.0Cr. *J. Manuf. Process.* **2023**, *97*, 35–47. [\[CrossRef\]](#)
80. Agrawal, C.; Khanna, N.; Gupta, M.K.; Kaynak, Y. Sustainability assessment of in-house developed environment-friendly hybrid techniques for turning Ti-6Al-4V. *Sustain. Mater. Technol.* **2020**, *26*, e00220. [\[CrossRef\]](#)
81. Hassan, A.; Khan, M.A.; Younas, M.; Jaffery, S.H.I.; Khan, M.; Ahmed, N.; Awang, M. Impact of dry and cryogenic cutting medium on shear angle and chip morphology in high-speed machining of titanium alloy (Ti-6Al-4V). *Int. J. Automot. Mech. Eng.* **2024**, *21*, 11316–11331. [\[CrossRef\]](#)
82. Li, K.; Shao, W.; Tang, J.; Huang, W.; Li, X. Feasibility study of high feed axial ultrasonic vibration turning of Ti6Al4V. *Arch. Civ. Mech. Eng.* **2024**, *24*, 137. [\[CrossRef\]](#)
83. Airao, J.; Nirala, C.K.; Outeiro, J.; Khanna, N. Surface integrity in ultrasonic-assisted turning of Ti6Al4V using sustainable cutting fluid. *Procedia CIRP* **2022**, *108*, 55–60. [\[CrossRef\]](#)
84. Kandi, R.; Sahoo, S.K.; Sahoo, A.K. Ultrasonic vibration-assisted turning of Titanium alloy Ti-6Al-4V: Numerical and experimental investigations. *J. Braz. Soc. Mech. Sci. Eng.* **2020**, *42*, 399. [\[CrossRef\]](#)
85. Pei, L.; Wu, H. Effect of ultrasonic vibration on ultra-precision diamond turning of Ti6Al4V. *Int. J. Adv. Manuf. Technol.* **2019**, *103*, 433–440. [\[CrossRef\]](#)
86. Zhang, J.; Wang, D. Investigations of tangential ultrasonic vibration turning of Ti6Al4V using finite element method. *Int. J. Mater. Form.* **2019**, *12*, 257–267. [\[CrossRef\]](#)
87. Sui, H.; Zhang, X.; Zhang, D.; Jiang, X.; Wu, R. Feasibility study of high-speed ultrasonic vibration cutting titanium alloy. *J. Mech. Work. Technol.* **2017**, *247*, 111–120. [\[CrossRef\]](#)

88. Sivareddy, D.V.; Krishna, P.V.; Gopal, A.V. Experimental investigation on flank wear of the tool in ultrasonic vibration-assisted turning of Ti6Al4V alloy. *Smart Sustain. Manuf. Syst.* **2021**, *5*, 101–112. [\[CrossRef\]](#)
89. Olt, J.; Maksarov, V.V.; Efimov, A.E. Improving the surface quality of titanium-alloy components in machining. *Russ. Eng. Res.* **2023**, *43*, 195–198. [\[CrossRef\]](#)
90. Liu, X.; Shan, C.; Xiong, Y.; Zhou, C. Modeling and simulation for orthogonal cutting force in ultrasonic vibration-assisted machining in situ TiB2/Al MMCs. *Int. J. Adv. Manuf. Technol.* **2025**, *137*, 1667–1682. [\[CrossRef\]](#)
91. Du, P.; Han, L.; Qiu, X.; Chen, W.; Deng, J.; Liu, Y.; Zhang, J. Development of a high-precision piezoelectric ultrasonic milling tool using longitudinal-bending hybrid transducer. *Int. J. Mech. Sci.* **2022**, *222*, 107239. [\[CrossRef\]](#)
92. Baraya, M.; Yan, J.; Hossam, M. Improving and predicting the surface roughness and the machining accuracy in ultrasonic vibration-assisted milling. *J. Vib. Eng. Technol.* **2024**, *12*, 127–140. [\[CrossRef\]](#)
93. Wang, X.; Zhuang, B.; Wu, T.; Su, H.; Chen, Y.; Zhao, B.; Ding, W. Microstructure evolution characterization of Ti2AlNb intermetallic alloys subjected to side milling. *Mater. Today Commun.* **2025**, *42*, 111257. [\[CrossRef\]](#)
94. Sun, J.; Li, P.; Zhang, S.; Chen, Y.; Lu, H.; Chen, G.; Shao, D. Experimental study of surface integrity in ultrasonic vibration-assisted milling of GH4169 nickel-based superalloy. *Int. J. Adv. Manuf. Technol.* **2023**, *129*, 5047–5058. [\[CrossRef\]](#)
95. Gu, G.; Wu, S.; Wang, D.; Zhou, S.; Zhu, L.; An, Q.; Guo, H.; Li, C. A review of the research on the variation of tool's motion trajectory and its influence on the formation mechanism of surface quality in ultrasonic vibration machining. *J. Manuf. Process.* **2023**, *107*, 294–319. [\[CrossRef\]](#)
96. Song, Y.; Wang, Z.; Huang, L. Study on surface quality and tool wear of TiAl alloy in ultrasonic longitudinal torsion assisted milling. *Manuf. Technol. Mach. Tool* **2024**, *2*, 31–37. [\[CrossRef\]](#)
97. Gao, G.; Xiang, Y.; Qiao, H.; Wei, C.; Wang, G.; Xiang, D. Modeling on cutting force considering tool flank wear in ultrasonic vibration-assisted milling Ti3Al. *Wear* **2025**, *566–567*, 205761. [\[CrossRef\]](#)
98. Wang, B.; Tang, M.; Song, C.; Wang, H.; Long, Z.; Xu, R. Effects of shear thickening fluid preparation on tool performance in the milling of Ti6Al4V titanium alloy. *J. Manuf. Process.* **2024**, *113*, 95–104. [\[CrossRef\]](#)
99. Wang, F.; Pang, Q.; Yang, Q.; Han, H. Effect of cryogenic cooling on micro-milling properties of titanium alloy. *J. Mater. Eng. Perform.* **2024**, *34*, 6472–6483. [\[CrossRef\]](#)
100. Wang, Q.; Chen, X.; An, Q.; Chen, M.; Guo, H.; He, Y. Research on cutting performance and tool life improvement methods of titanium alloy ultra-high speed milling tools. *J. Manuf. Process.* **2024**, *131*, 38–51. [\[CrossRef\]](#)
101. Xie, W.; Wang, X.; Liu, E.; Wang, J.; Tang, X.; Li, G.; Zhang, J.; Yang, L.; Chai, Y.; Zhao, B. Research on cutting force and surface integrity of TC18 titanium alloy by longitudinal ultrasonic vibration assisted milling. *Int. J. Adv. Manuf. Technol.* **2022**, *119*, 4745–4755. [\[CrossRef\]](#)
102. Ni, C.; Zhu, L.; Yang, Z. Comparative investigation of tool wear mechanism and corresponding machined surface characterization in feed-direction ultrasonic vibration assisted milling of Ti-6Al-4V from dynamic view. *Wear* **2019**, *436*, 203006. [\[CrossRef\]](#)
103. Gao, G.; Xia, Z.; Su, T.; Xiang, D.; Zhao, B. Cutting force model of longitudinal-torsional ultrasonic-assisted milling Ti-6Al-4V based on tool flank wear. *J. Mech. Work. Technol.* **2021**, *291*, 117042. [\[CrossRef\]](#)
104. Xie, W.; Zhao, B.; Liu, E.; Chai, Y.; Wang, X.; Yang, L.; Li, G.; Wang, J. Surface integrity investigation into longitudinal-torsional ultrasonic vibration side milling for a TC18 titanium alloy—Part I: The effects of cutting speed on cutting force and surface integrity. *Int. J. Adv. Manuf. Technol.* **2022**, *120*, 2701–2713. [\[CrossRef\]](#)
105. Hu, W.; Du, P.; Qiu, X.; Zhao, X.; Hu, Z.; Zhang, J.; Liu, Y. Enhanced dry machinability of TC4 titanium alloy by longitudinal-bending hybrid ultrasonic vibration-assisted milling. *J. Clean. Prod.* **2022**, *379*, 134866. [\[CrossRef\]](#)
106. Ren, W.; Xu, J.; Lin, J.; Yu, Z.; Yu, P.; Lian, Z.; Yu, H. Research on homogenization and surface morphology of Ti-6Al-4V alloy by longitudinal-torsional coupled ultrasonic vibration ball-end milling. *Int. J. Adv. Manuf. Technol.* **2019**, *104*, 301–313. [\[CrossRef\]](#)
107. Ying, N.; Feng, J.; Bo, Z. A novel 3D finite element simulation method for longitudinal-torsional ultrasonic-assisted milling. *Int. J. Adv. Manuf. Technol.* **2020**, *106*, 385–400. [\[CrossRef\]](#)
108. Liu, Q.; Xu, J.; Yu, H. Experimental study of tool wear and its effects on cutting process of ultrasonic-assisted milling of Ti6Al4V. *Int. J. Adv. Manuf. Technol.* **2020**, *108*, 2917–2928. [\[CrossRef\]](#)
109. Su, Y.; Li, L. Surface integrity of ultrasonic-assisted dry milling of SLM Ti6Al4V using polycrystalline diamond tool. *Int. J. Adv. Manuf. Technol.* **2022**, *119*, 5947–5956. [\[CrossRef\]](#)
110. Chen, P.; Tong, J.; Zhao, J.; Zhang, Z.; Zhao, B. A study of the surface microstructure and tool wear of titanium alloys after ultrasonic longitudinal-torsional milling. *J. Manuf. Process.* **2020**, *53*, 1–11. [\[CrossRef\]](#)
111. Zheng, K.; Liao, W.; Dong, Q.; Sun, L. Friction and wear on titanium alloy surface machined by ultrasonic vibration-assisted milling. *J. Braz. Soc. Mech. Sci. Eng.* **2018**, *40*, 411. [\[CrossRef\]](#)
112. Lu, W.; Ni, C.; Wang, Y.; Zong, C.; Liu, D. Micromachining performance of additively manufactured titanium alloys in synergistic application of ultrasonic elliptical machining and textured tool methods. *Int. J. Adv. Manuf. Technol.* **2025**, *136*, 2707–2729. [\[CrossRef\]](#)

113. Chang, B.; Yi, Z.; Cao, X.; Duan, J.-A. Surface feature and material removal in ultrasonic vibration-assisted slot-milling of Ti-6Al-4V titanium alloy. *Int. J. Adv. Manuf. Technol.* **2022**, *122*, 2235–2251. [\[CrossRef\]](#)
114. Niu, Q.; Rong, J.; Jing, L.; Gao, H.; Tang, S.; Qiu, X.; Liu, L.; Wang, X.; Dai, F. Study on force-thermal characteristics and cutting performance of titanium alloy milled by ultrasonic vibration and minimum quantity lubrication. *J. Manuf. Process.* **2023**, *95*, 115–130. [\[CrossRef\]](#)
115. Li, G.; Xie, W.; Wang, H.; Chai, Y.; Zhang, S.; Yang, L. Optimizing processing parameters and surface quality of TC18 via ultrasonic-assisted milling (UAM): An experimental study. *Micromachines* **2023**, *14*, 1111. [\[CrossRef\]](#) [\[PubMed\]](#)
116. Lü, Q.; Yang, S.; Yang, L.; Liu, E.; Li, G.; Xiang, D. Optimization milling force and surface roughness of Ti-6Al-4V based on ultrasonic-assisted milling (UAM): An experimental study. *Micromachines* **2023**, *14*, 1699. [\[CrossRef\]](#) [\[PubMed\]](#)
117. Qin, S.; Zhu, L.; Wiercigroch, M.; Ren, T.; Hao, Y.; Ning, J.; Zhao, J. Material removal and surface generation in longitudinal-torsional ultrasonic assisted milling. *Int. J. Mech. Sci.* **2022**, *227*, 107375. [\[CrossRef\]](#)
118. Gao, H.; Ma, B.; Zhu, Y.; Yang, H. Enhancement of machinability and surface quality of Ti-6Al-4V by longitudinal ultrasonic vibration-assisted milling under dry conditions. *Measurement* **2022**, *187*, 110324. [\[CrossRef\]](#)
119. Ming, W.; Cai, C.; Ma, Z.; Nie, P.; Li, C.; An, Q. Milling mechanism and surface roughness prediction model in ultrasonic vibration-assisted side milling of Ti-6Al-4V. *Int. J. Adv. Manuf. Technol.* **2024**, *131*, 2279–2293. [\[CrossRef\]](#)
120. Rinck, P.M.; Gueray, A.; Zaeh, M.F. Modeling of cutting forces in 1-D and 2-D ultrasonic vibration-assisted milling of Ti-6Al-4V. *Int. J. Adv. Manuf. Technol.* **2022**, *119*, 1807–1819. [\[CrossRef\]](#)
121. Outeiro, J.; Cheng, W.; Chinesta, F.; Ammar, A. Modelling and optimization of machining of Ti-6Al-4V titanium alloy using machine learning and design of experiments methods. *J. Manuf. Mater. Process.* **2022**, *6*, 58. [\[CrossRef\]](#)
122. García-Martínez, E.; Miguel, V.; Martínez-Martínez, A. Economic analysis of eco-friendly lubrication strategies for the machining of Ti48Al2Cr2Nb aluminide. *J. Clean. Prod.* **2024**, *435*, 140541. [\[CrossRef\]](#)
123. García-Martínez, E.; Miguel, V.; Martínez-Martínez, A. Effect of minimum quantity of lubricant on carbide tools and surface integrity in the machining of titanium aluminides. *Metals* **2024**, *14*, 399. [\[CrossRef\]](#)
124. Feng, R.; Shao, Z.; Yang, S.; Cao, H.; Li, H.; Lei, C.; Zhang, J. Material removal behavior of nanoscale shear cutting and extrusion cutting of monocrystalline γ -TiAl alloy. *Int. J. Adv. Manuf. Technol.* **2022**, *119*, 6729–6742. [\[CrossRef\]](#)
125. Rauf, A.; Khan, M.A.; Jaffery, S.H.I.; Butt, S.I. Effects of machining parameters, ultrasonic vibrations and cooling conditions on cutting forces and tool wear in meso scale ultrasonic vibrations assisted end-milling (UVAEM) of Ti-6Al-4V under dry, flooded, MQL and cryogenic environments—A statistical analysis. *J. Mater. Res. Technol.* **2024**, *30*, 8287–8303. [\[CrossRef\]](#)
126. Khan, A.A.; Ahmed, M.I. Improving tool life using cryogenic cooling. *J. Mech. Work. Technol.* **2008**, *196*, 149–154. [\[CrossRef\]](#)
127. Korkmaz, M.E.; Gupta, M.; Ross, N.S.; Sivalingam, V. Implementation of green cooling/lubrication strategies in metal cutting industries: A state of the art towards sustainable future and challenges. *Sustain. Mater. Technol.* **2023**, *36*, e00641. [\[CrossRef\]](#)
128. Sun, S.; Brandt, M.; Palanisamy, S.; Dargusch, M.S. Effect of cryogenic compressed air on the evolution of cutting force and tool wear during machining of Ti-6Al-4V alloy. *J. Mech. Work. Technol.* **2015**, *221*, 243–254. [\[CrossRef\]](#)
129. Li, L.; Zhang, Y.; Mu, J.; Xu, J.; Zhao, J.; Li, P.; Liu, Z. Analysis of machinability in milling of high-strength brittle thin plates of γ -TiAlNb intermetallic compound. *J. Mech. Sci. Technol.* **2024**, *38*, 4085–4095. [\[CrossRef\]](#)
130. Li, H.; Zhu, H.; Zhou, B.; Chen, Y.; Feng, R.; Cao, H.; Lei, C. Effect of structure tool on nano-cutting surface integrity of single crystal γ -TiAl alloy via atomic simulation. *Mater. Today Commun.* **2024**, *40*, 110034. [\[CrossRef\]](#)
131. Bermingham, M.; Palanisamy, S.; Kent, D.; Dargusch, M. A comparison of cryogenic and high pressure emulsion cooling technologies on tool life and chip morphology in Ti-6Al-4V cutting. *J. Mech. Work. Technol.* **2012**, *212*, 752–765. [\[CrossRef\]](#)
132. Fan, G.; Zhang, J.; Chen, H.; Xiao, G.; Chen, Z.; Yi, M.; Xu, C.; Fan, L.; Li, G. Analysis of tool wear of TiAlN coated tool, machined surface morphology and chip during titanium alloy milling. *Tribol. Int.* **2024**, *197*, 109751. [\[CrossRef\]](#)
133. Zareena, A.; Veldhuis, S. Tool wear mechanisms and tool life enhancement in ultra-precision machining of titanium. *J. Mech. Work. Technol.* **2012**, *212*, 560–570. [\[CrossRef\]](#)
134. Zhang, C.; Xu, J.; Geng, X.; Wang, Z. Simulation Study on Cutting Titanium Alloy with Micro-Textured tool. In Proceedings of the 2024 IEEE International Conference on Manipulation, Manufacturing and Measurement on the Nanoscale (3M-NANO), Zhongshan, China, 29 July–2 August 2024; IEEE: New York, NY, USA; pp. 24–28. [\[CrossRef\]](#)
135. Ma, J.; Zhang, Y.; Jiao, F.; Cui, X.; Zhang, D.; Ren, L.; Zhao, B.; Pang, X. Dynamic milling force model considering vibration and tool flank wear width for monitoring tool states in machining of Ti-6Al-4V. *J. Manuf. Process.* **2024**, *124*, 1519–1540. [\[CrossRef\]](#)
136. Wang, Z.; Liu, Y. Study of surface integrity of milled gamma titanium aluminide. *J. Manuf. Process.* **2020**, *56*, 806–819. [\[CrossRef\]](#)
137. Priarone, P.C.; Rizzuti, S.; Rotella, G.; Settineri, L. Tool wear and surface quality in milling of a gamma-TiAl intermetallic. *Int. J. Adv. Manuf. Technol.* **2012**, *61*, 25–33. [\[CrossRef\]](#)
138. Zhang, Y.; Zhang, Q.; Zhao, J.; Zhu, Y.; Fu, X.; Yang, C.; Chen, Y. Ultrasonic vibration assisted milling of titanium alloy microchannel. *Precis. Eng.* **2024**, *88*, 251–265. [\[CrossRef\]](#)

139. Wang, Y.; Gao, G.; Zhang, K.; Wang, Y.; Wang, X.; Xiang, D. Modelling of tribological behavior and wear for micro-textured surfaces of Ti2AlNb intermetallic compounds machined with multi-dimensional ultrasonic vibration assistance. *Tribol. Int.* **2024**, *191*, 109167. [\[CrossRef\]](#)
140. Wu, S.; Chen, F.; Wang, D.; Wang, G.; Li, C.; Lu, J. Machining mechanism and stress model in cutting Ti6Al4V. *Int. J. Adv. Manuf. Technol.* **2024**, *131*, 2625–2639. [\[CrossRef\]](#)
141. Wang, X.; Wang, J.; Oiu, W.; Niu, J.; Fu, X.; Qiao, Y. Material removal mechanism and surface integrity of cutting titanium aluminum alloy under different cooling conditions. *Acta Aeronaut. Astronaut. Sin.* **2024**, *45*, 629471. [\[CrossRef\]](#)
142. Yang, P.; Li, X.; Zhang, X.; Yao, Z.; Shivpuri, R. Improved dynamic recrystallization modeling in the high-speed machining of titanium alloy. *Int. J. Adv. Manuf. Technol.* **2024**, *130*, 2563–2586. [\[CrossRef\]](#)
143. Hussain, A.; Layegh, S.E.; Lazoglu, I.; Arrazola, P.-J.; Lazcano, X.; Aristimuño, P.-X.; Subasi, O.; Yigit, I.E.; Öztürk, Ç.; Yavaş, Ç. Mechanics of milling 48-2-2 gamma titanium aluminide. *CIRP J. Manuf. Sci. Technol.* **2020**, *30*, 131–139. [\[CrossRef\]](#)
144. Hukkerikar, A. Milling of Gamma titanium aluminides. *ebiltegia* **2022**, 1–225. [\[CrossRef\]](#)
145. Guo, S.; Du, W.; Jiang, Q.; Dong, Z.; Zhang, B. Surface integrity of ultrasonically-assisted milled Ti6Al4V alloy manufactured by selective laser melting. *Chin. J. Mech. Eng.* **2021**, *34*, 67. [\[CrossRef\]](#)
146. Yin, J.; Sun, R.; Ming, C.; Chen, C.; Zeng, S. Investigation of single grain grinding of Titanium Alloy using Diamond Abrasive Grain with positive rake Angle. *Machines* **2024**, *12*, 451. [\[CrossRef\]](#)
147. Li, Z.; Yang, S.; Liu, X.; Xiao, G.; San, H.; Zhang, Y.; Wang, W.; Yang, Z. Grinding force model for ultrasonic assisted grinding of γ -TiAl intermetallic compounds and experimental validation. *Rev. Adv. Mater. Sci.* **2024**, *63*, 20230167. [\[CrossRef\]](#)
148. Ni, M.J.; Liu, R.C.; Zhou, H.H.; Yang, C.; Ge, S.Y.; Liu, D.; Shi, F.L.; Cui, Y.Y.; Yang, R. Influence of Grinding Depth on the Surface Integrity and Fatigue Property of γ -TiAl Alloy. *Acta Metall. Sin.* **2022**, *60*, 261–272. [\[CrossRef\]](#)
149. Chen, T.; Wang, X.; Zhao, B.; Ding, W.; Xiong, M.; Xu, J.; Liu, Q.; Xu, D.; Zhao, Y.; Zhu, J. Material removal mechanisms in ultrasonic vibration-assisted high-efficiency deep grinding γ -TiAl alloy. *Chin. J. Aeronaut.* **2024**, *37*, 462–476. [\[CrossRef\]](#)
150. Wang, X.; Tang, Y.; Zhao, B.; Chen, T.; Ding, W.; Xu, J. Grindability of γ -TiAl intermetallic compounds during ultrasonic vibration-assisted high efficiency deep grinding process. *Int. J. Adv. Manuf. Technol.* **2023**, *128*, 1127–1138. [\[CrossRef\]](#)
151. Zhao, B.; Wang, X.; Chen, T.; Ding, W.; Qian, N.; Xu, J. Simulation and experimental thermal analysis of ultrasonic vibration-assisted high-efficiency deep grinding of γ -TiAl blade tenon. *Appl. Therm. Eng.* **2025**, *258*, 124629. [\[CrossRef\]](#)
152. Bhaduri, D.; Soo, S.L.; Aspinwall, D.K.; Novovic, D.; Bohr, S.; Harden, P.; Webster, J.A. Ultrasonic assisted creep feed grinding of gamma titanium aluminide using conventional and superabrasive wheels. *CIRP Ann.* **2017**, *66*, 341–344. [\[CrossRef\]](#)
153. Cao, Y.; Zhu, Y.; Li, H.N.; Wang, C.; Su, H.; Yin, Z.; Ding, W. Development and performance of a novel ultrasonic vibration plate sonotrode for grinding. *J. Manuf. Process.* **2020**, *57*, 174–186. [\[CrossRef\]](#)
154. Nik, M.G.; Movahhedy, M.R.; Akbari, J. Ultrasonic-assisted grinding of Ti6Al4 V alloy. *Procedia CIRP* **2012**, *1*, 353–358. [\[CrossRef\]](#)
155. Wu, H.; Ye, X.; Chen, Z.; Zhang, S.; Zeng, J.; Wang, Q.; Wu, Y. Reducing wheel loading in the grinding of titanium alloys through ultrasonic-assisted plasma oxidation modification. *Lubricants* **2023**, *11*, 397. [\[CrossRef\]](#)
156. Liu, J.; Liu, Z.; Yan, Y.; Wang, X. Study on the CBN wheel wear mechanism of longitudinal-torsional ultrasonic-assisted grinding applied to TC4 titanium alloy. *Micromachines* **2022**, *13*, 1480. [\[CrossRef\]](#) [\[PubMed\]](#)
157. Zhao, B.; Guo, X.; Bie, W.; Chang, B.; Zhao, C. Thermo-mechanical coupling effect on surface residual stress during ultrasonic vibration-assisted forming grinding gear. *J. Manuf. Process.* **2020**, *59*, 19–32. [\[CrossRef\]](#)
158. Li, B.; Dai, C.; Ding, W.; Yang, C.; Li, C.; Kulik, O.; Shumyacher, V. Prediction on grinding force during grinding powder metallurgy nickel-based superalloy FGH96 with electroplated CBN abrasive wheel. *Chin. J. Aeronaut.* **2021**, *34*, 65–74. [\[CrossRef\]](#)
159. Song, J.; Zhao, B.; Ding, W.; Zhao, Y.; Zhu, J.; Cui, H. Wear mechanism of aggregated cBN grains during single-grain ultrasonic vibration-assisted grinding of γ -TiAl alloys. *Int. J. Adv. Manuf. Technol.* **2024**, *135*, 4749–4764. [\[CrossRef\]](#)
160. Prastyo, D.T.; Andoko; Puspitasari, P.; Prasetya, R. Recent progress and applications of coolant-lubricants in titanium machining: A review. *AIP Conf. Proc.* **2024**, *2991*, 020032.
161. Ramírez-Ramírez, J.H.; Pineda-Arriaga, K.Y.; Gaona-Martínez, M.J.; Benavides-Treviño, J.R.; Pérez-González, F.A.; Colás, R.; Garza-Montes-De-Oca, N.F. The Role of Heat Treatment in the Wear Behavior of a γ -TiAl Alloy under Dry Sliding Conditions. *J. Mater. Eng. Perform.* **2025**, *34*, 1–12. [\[CrossRef\]](#)
162. Ren, Z.; Feng, R.; Cao, H.; Zhou, B.; Li, H.; Lei, C. Wear mechanism of diamond-cutting tool in nano-cutting polycrystalline γ -TiAl alloy based on molecular dynamics simulation. *J. Manuf. Process.* **2024**, *119*, 118–129. [\[CrossRef\]](#)
163. Vashishtha, G.; Chauhan, S.; Gupta, M.K.; Korkmaz, M.E.; Ross, N.S.; Zimroz, R.; Krolczyk, G.M. Configuration of tool wear and its mechanism in sustainable machining of titanium alloys with energy signals. *Int. J. Adv. Manuf. Technol.* **2024**, *134*, 3561–3573. [\[CrossRef\]](#)
164. Kuo, C.; Hsu, Y.; Chung, C.; Chen, C.-C.A. Multiple criteria optimisation in coated abrasive grinding of titanium alloy using minimum quantity lubrication. *Int. J. Mach. Tools Manuf.* **2017**, *115*, 47–59. [\[CrossRef\]](#)
165. Zhu, L.; Qin, S.; Hao, Y.; Yan, T.; Yang, Z.; Yong, J.; Shu, X. Knowledge-based intelligent ensemble monitoring method of grit wear in ultrasonic assisted grinding. *Adv. Eng. Inform.* **2025**, *64*, 103043. [\[CrossRef\]](#)

166. Chen, T.; Wang, X.; Zhao, B.; Ding, W.; Xu, J. Surface integrity evolution during creep feed profile grinding of γ -TiAl blade tenon. *Chin. J. Aeronaut.* **2024**, *37*, 496–512. [\[CrossRef\]](#)
167. Yan, Y.; Zhang, Q.; Ma, Q.; Yuan, D. Research of the surface residual stress of TC4 titanium alloy under longitudinal-torsional ultrasonic grinding and nanofluid minimum quantity lubrication. *Int. J. Adv. Manuf. Technol.* **2024**, *138*, 2297–2311. [\[CrossRef\]](#)
168. Xia, Z.; Shan, C.; Zhang, M.; Liu, W.; Cui, M.; Luo, M. Machinability of elliptical ultrasonic vibration milling γ -TiAl: Chip formation, edge breakage, and subsurface layer deformation. *Chin. J. Aeronaut.* **2025**, *38*, 103096. [\[CrossRef\]](#)
169. Rotella, G.; Imbrogno, S.; Candamano, S.; Umbrello, D. Surface integrity of machined additively manufactured Ti alloys. *J. Mech. Work. Technol.* **2018**, *259*, 180–185. [\[CrossRef\]](#)
170. Schneider, F.; Lohkamp, R.; Sousa, F.; Müller, R.; Aurich, J. Analysis of the surface integrity in ultra-precision cutting of cp-titanium by investigating the chip formation. *Procedia CIRP* **2014**, *13*, 55–60. [\[CrossRef\]](#)
171. Shen, J.; Wang, L.; Cao, Z.; Hu, L. Synergistically enhanced strength and ductility in TiAl/Nb composites via core-shell structure design. *Mater. Sci. Eng. A* **2024**, *918*, 147417. [\[CrossRef\]](#)
172. Paillard, M.; Rossi, F.; Elias-Birembaux, H.; Poulachon, G.; Ritou, M.; Maury, N. Effects of the Tool Microgeometry on Thermo-Mechanical Loads for Ti-6Al-4V Finishing Cutting Operations. *Procedia CIRP* **2025**, *133*, 442–447. [\[CrossRef\]](#)
173. Malkin, S.; Guo, C. *Grinding technology: Theory and Application of Machining with Abrasives*; Industrial Press Inc.: New York, NY, USA, 2008.
174. Singh, R.; Dureja, J.; Dogra, M.; Gupta, M.K.; Jamil, M.; Mia, M. Evaluating the sustainability pillars of energy and environment considering carbon emissions under machining of Ti-3Al-2.5 V. *Sustain. Energy Technol. Assess.* **2020**, *42*, 100806. [\[CrossRef\]](#)
175. Liang, Y.; Lin, J. Fabrication and properties of γ -TiAl sheet materials: A review. *JOM* **2017**, *69*, 2571–2575. [\[CrossRef\]](#)
176. Sitharaj, A.; Arulmurugan, B.; Balaji, D.; Idhayaraja, S. Additive Manufacturing of Titanium-based Alloys by Wire Arc Directed Energy Deposition (WA-DED): A Review. In *Advances in Solid-State Welding and Processing of Metallic Materials*; Taylor & Francis: London, UK, 2025. [\[CrossRef\]](#)
177. Soori, M.; Jough, F.K.G. Internal cooling system effects to heat transfer and tool wear in turning operations of titanium alloys Ti6Al4V. *Trans. Can. Soc. Mech. Eng.* **2024**, *49*, 118–127. [\[CrossRef\]](#)
178. Li, A.; Zhang, X.; Chen, J.; Shi, T.; Wen, L.; Yu, T. Review of ultrasonic vibration-assisted milling technology. *Precis. Eng.* **2024**, *91*, 601–616. [\[CrossRef\]](#)
179. Hsu, C.Y.; Huang, C.K.; Wu, C.Y. Milling of MAR-M247 nickel-based superalloy with high temperature and ultrasonic aiding. *Int. J. Adv. Manuf. Technol.* **2007**, *34*, 857–866. [\[CrossRef\]](#)
180. Wang, B.S.; Zuo, J.M.; Wang, M.L.; Hou, J.M. Prediction of milling force based on numerical simulation of oblique cutting. *Mater. Manuf. Process.* **2012**, *27*, 1011–1016. [\[CrossRef\]](#)
181. Aydın, M.; Uçar, M.; Cengiz, A.; Kurt, M.; Bakır, B. A methodology for cutting force prediction in side milling. *Mater. Manuf. Process.* **2014**, *29*, 1429–1435. [\[CrossRef\]](#)
182. Palanikumar, K.; Boppana, S.; Natarajan, E. Analysis of chip formation and temperature measurement in machining of titanium alloy (Ti-6Al-4V). *Exp. Tech.* **2023**, *47*, 517–529. [\[CrossRef\]](#)
183. Niu, Y.; Jiao, F.; Zhao, B.; Gao, G. Investigation of cutting force in longitudinal-torsional ultrasonic-assisted milling of Ti-6Al-4V. *Materials* **2019**, *12*, 1955. [\[CrossRef\]](#)
184. Bao, W.; Tansel, I. Modeling micro-end-milling operations. Part I: Analytical cutting force model. *Int. J. Mach. Tools Manuf.* **2000**, *40*, 2155–2173. [\[CrossRef\]](#)
185. Bissacco, G.; Hansen, H.; Slunsky, J. Modelling the cutting edge radius size effect for force prediction in micro milling. *CIRP Ann.* **2008**, *57*, 113–116. [\[CrossRef\]](#)
186. Chen, N.; Li, L.; Wu, J.M.; Qian, J.; He, N.; Reynaerts, D. Research on the ploughing force in micro milling of soft-brittle crystals. *Int. J. Mech. Sci.* **2019**, *155*, 315–322. [\[CrossRef\]](#)
187. Werner, G. Influence of work material on grinding forces. *Ann. CIRP* **1978**, *27*, 243–248.
188. Chiu, N.; Malkin, S. Computer simulation for cylindrical plunge grinding. *CIRP Ann.* **1993**, *42*, 383–387. [\[CrossRef\]](#)
189. Guo, M.; Li, B. A frequency-domain grinding force model-based approach to evaluate the dynamic performance of high-speed grinding machine tools. *Mach. Sci. Technol.* **2016**, *20*, 115–131. [\[CrossRef\]](#)
190. Guo, M.; Li, B.; Ding, Z.; Liang, S.Y. Empirical modeling of dynamic grinding force based on process analysis. *Int. J. Adv. Manuf. Technol.* **2016**, *86*, 3395–3405. [\[CrossRef\]](#)
191. Guo, M.; Jiang, X.; Ding, Z.; Wu, Z. A frequency domain dynamic response approach to optimize the dynamic performance of grinding machine spindles. *Int. J. Adv. Manuf. Technol.* **2018**, *98*, 2737–2745. [\[CrossRef\]](#)
192. Lindvall, R.; Lenrick, F.; Andersson, J.M.; M'SAoubi, R.; Bushlya, V. On wear of TiAlN coated tools with and without NbN overlayer in machining titanium alloys. *Int. J. Mach. Tools Manuf.* **2024**, *198*, 104148. [\[CrossRef\]](#)
193. Cao, H.; Huang, Q.; Xu, H.; Zhou, B.; Chen, W.; Yu, M.; Feng, R. Effect of aqueous layer thickness on nano-scratching of single-crystal γ -TiAl alloys. *Mol. Simul.* **2024**, *50*, 1076–1091. [\[CrossRef\]](#)

194. Zhao, J.; Huang, J.; Xiang, Y.; Wang, R.; Xu, X.; Ji, S.; Hang, W. Effect of a protective coating on the surface integrity of a microchannel produced by microultrasonic machining. *J. Manuf. Process.* **2021**, *61*, 280–295. [\[CrossRef\]](#)
195. Lan, T.; Feng, P.; Zhang, J.; Zhang, X.; Zheng, Z.; Wang, J. Experimental investigation on the combined effects of mechano-chemical and ultrasonic vibration in titanium alloy grinding. *J. Manuf. Process.* **2024**, *121*, 382–393. [\[CrossRef\]](#)
196. Yoon, H.-S.; Kwon, S.B.; Kim, J.-H.; Ahn, S.-H.; Min, S. Effects of surface coating materials on cutting forces and ductile-to-brittle transition in orthogonal cutting of monocrystalline sapphire. *J. Manuf. Process.* **2022**, *84*, 375–382. [\[CrossRef\]](#)
197. Wu, H.; Duan, W.; Sun, L.; Zeng, J.; Li, S.; Wang, Q.; Wu, Y.; Chen, Y. Effect of ultrasonic vibration on the machining performance and mechanism of hybrid ultrasonic vibration/plasma oxidation assisted grinding. *J. Manuf. Process.* **2023**, *94*, 466–478. [\[CrossRef\]](#)
198. Wu, H.; Ye, X.; Liao, Z.; Li, S.; Xiao, C.; Zeng, J.; Zhang, S.; Wu, Y. Machinability improvement of titanium alloy in face grinding by ultrasonic assisted jet plasma oxidation. *Chin. J. Aeronaut.* **2025**, *38*, 103130. [\[CrossRef\]](#)
199. Zhang, C.; Cao, Y.; Jiao, F.; Wang, J. Research on cutting force characteristics of laser ultrasonically assisted turning of cemented carbide. *Int. J. Refract. Met. Hard Mater.* **2024**, *122*, 106726. [\[CrossRef\]](#)
200. Dominguez-Caballero, J.; Ayvar-Soberanis, S.; Kim, J.; Roy, A.; Li, L.; Curtis, D. Hybrid simultaneous laser- and ultrasonic-assisted machining of Ti-6Al-4V alloy. *Int. J. Adv. Manuf. Technol.* **2023**, *125*, 1903–1916. [\[CrossRef\]](#)
201. Goigana, M.; Sarasua, J.; Ramos, J.; Echavarri, L.; Cascón, I. Pulsed ultrasonic assisted electrical discharge machining for finishing operations. *Int. J. Mach. Tools Manuf.* **2016**, *109*, 87–93. [\[CrossRef\]](#)
202. Bhargav, K.V.J.; Balaji, P.S.; Sahu, R.K.; Leblouba, M. Experimental investigation on machining characteristics of titanium processed using electrolyte sonicated μ -ECDM system. *Sci. Rep.* **2022**, *12*, 15540. [\[CrossRef\]](#)
203. Xing, Y.; Liu, Y.; Yin, T.; Li, D.; Sun, Z.; Xue, C.; Yip, W.S.; To, S. Magnetic and ultrasonic vibration dual-field assisted ultra-precision diamond cutting of high-entropy alloys. *Int. J. Mach. Tools Manuf.* **2024**, *202*, 104208. [\[CrossRef\]](#)
204. Fan, T.; Yao, C.; Tan, L.; Cao, Y.; Sun, Y.; Tang, W. The influence of induction-assisted milling on the machining characteristics and surface integrity of γ -TiAl alloys. *J. Manuf. Process.* **2024**, *118*, 215–227. [\[CrossRef\]](#)
205. Yip, W.; To, S. Sustainable manufacturing of ultra-precision machining of titanium alloys using a magnetic field and its sustainability assessment. *Sustain. Mater. Technol.* **2018**, *16*, 38–46. [\[CrossRef\]](#)
206. Zhuang, K.; Wan, L.; Weng, J.; Wu, Z.; Zhang, Y.; Tian, C.; Yang, Y. A new elastic abrasive jet machining method for post-treatment of tool coatings: A case study on TiAlN coated tools for titanium machining. *Tribol. Int.* **2023**, *185*, 108533. [\[CrossRef\]](#)
207. Jamil, M.F.; Sahto, M.P.; Mehmood, A. Comprehensive study on high-performance machining (HPM) of Inconel-718: A review. *Int. J. Adv. Manuf. Technol.* **2025**, *139*, 5305–5337. [\[CrossRef\]](#)

Disclaimer/Publisher’s Note: The statements, opinions and data contained in all publications are solely those of the individual author(s) and contributor(s) and not of MDPI and/or the editor(s). MDPI and/or the editor(s) disclaim responsibility for any injury to people or property resulting from any ideas, methods, instructions or products referred to in the content.